

Tectonics

RESEARCH ARTICLE

10.1029/2020TC006300

Special Section:

Tethyan dynamics: from rifting to collision

Key Points:

- The upper plate of the Neotethys subduction system has been deformed by alternating episodes of compression and extension since the Cretaceous
- The alternating episodes of deformation are due to the episodes of advancing and retreating trench
- Numerical models simulate the episode of trench migration and upper-plate deformation by slab folding in the mantle transition zone

Supporting Information:

Supporting Information may be found in the online version of this article.

Correspondence to:






C. Faccenna,
claudio.faccenna@uniroma3.it

Citation:

Boutoux, A., Briaud, A., Faccenna, C., Ballato, P., Rossetti, F., & Blanc, E. (2021). Slab folding and surface deformation of the Iran mobile belt. *Tectonics*, 40, e2020TC006300. <https://doi.org/10.1029/2020TC006300>

Received 14 MAY 2020
 Accepted 21 MAY 2021

Slab Folding and Surface Deformation of the Iran Mobile Belt

Alexandre Boutoux¹ , Arthur Briaud^{1,2} , Claudio Faccenna^{1,3} , Paolo Ballato¹ , Federico Rossetti¹ , and Eric Blanc⁴

¹Department of Sciences, Roma Tre University, Rome, Italy, ²Observatoire de la Cote d'Azur, GeoAzur, CNRS Valbonne, France, ³Department of Geological Sciences, Jackson School of Geosciences, The University of Texas at Austin, Austin, TX, USA, ⁴Equinor AS, Exploration Research, Fornebu, Norway

Abstract Back-arc regions are usually punctuated by pulses of tectonic deformation, lasting for few tens of millions of years. Yet, the origin of those short-lived deformation episodes is disputed. Here, we compile structural, stratigraphic, geochemical, and geochronological data from Iran and we combine them with a kinematic reconstruction to show that the back-arc region of the Central Neotethys subduction zone was affected by alternating pulses of extension and compression, linked to episodes of trench retreat and advance, respectively. To back-up these observations and investigate the causes of such a trench behavior, we run 2D numerical models exploring (i) the dynamics of subduction into a viscously stratified mantle, and (ii) the deep slab deformation induced by mineral phase changes at the mantle transition zone. Our results indicate that episodes of trench retreat and trench advance, like those observed in the Central Neotethys domain, emerge spontaneously by slab folding, and penetration into the mantle transition zone. We propose a coupled mantle-surface tectonic evolution model of the Central Neotethys slab that reconciles back-arc deformation and short-lived pulses of upper-plate vertical motion in a unique, dynamically self-consistent model of deep mantle subduction.

1. Introduction

Back-arc systems record compressional and/or extensional deformation pulses lasting for a few tens of millions of years (e.g., Clark et al., 2008). This episodic and ephemeral style of upper-plate deformation has been documented in back-arc basins around the Western Pacific (e.g., Taylor & Karner, 1983), the Mediterranean (e.g., Faccenna et al., 2001; Guillaume et al., 2010; Hidas et al., 2013; Taylor & Karner, 1983), the Andes (e.g., De Celles et al., 2009; Martinod et al., 2013), and the Middle East (e.g., Agard et al., 2011).

Different models have been proposed so far to explain this discontinuous pattern of tectonic deformation, including subduction initiation (e.g., Gurnis et al., 2004), arrival of buoyant material at the trench (Martinod et al., 2013), change in the slab dip angle (e.g., Cramer et al., 2017; Dávila & Lithgow-Bertelloni, 2015), lateral slab tearing (e.g., Jolivet et al., 2013), or slab break-off (e.g., Agard et al., 2011; Wortel & Spakman, 2000). Another possible mechanism that may have an impact on the trench migration and hence on the tectonic regime of back-arc regions is represented by slab folding at the mantle transition zone (e.g., Cerpa et al., 2015; Guillaume et al., 2009; Gurnis & Hager, 1988; Ribe et al., 2007). This process is thought to generate periodic variations in both the slab dip angle and the trench motion that, in turn, may cause a switch in the mode of upper-plate deformation (Čížková et al., 2007; Ribe et al., 2007). Although this model has been proved to be physically feasible, its application to geological example is poorly documented. This is mostly because traces of ancient deformation are usually hidden by subsequent tectonic deformation. Here, we focus on the Iranian mobile belt, that is formed in the upper plate of the Tethyan subduction system along the Zagros convergence zone (Figure 1). Specifically, we take advantage of the increasing number of studies published over the last three decades to propose a regional tectonic reconstruction to unravel different episodes of Meso-Cenozoic deformation and relates it to the slab dynamics at depth.

The Iranian mobile belt is part of the Western Cimmerian Domain (WCD), which recorded a long-lasting tectonic history that includes terranes accretion against the Eurasian plate following the early Mesozoic Paleo-Tethys ocean suturing (e.g., Zanchi et al., 2006, 2009) and the early-middle Mesozoic to Paleogene oceanic subduction of the Neotethys culminating with the final collision between Arabia and Eurasia (e.g., Agard et al., 2011). Throughout the Mesozoic and the Cenozoic, the WCD recorded upper-plate

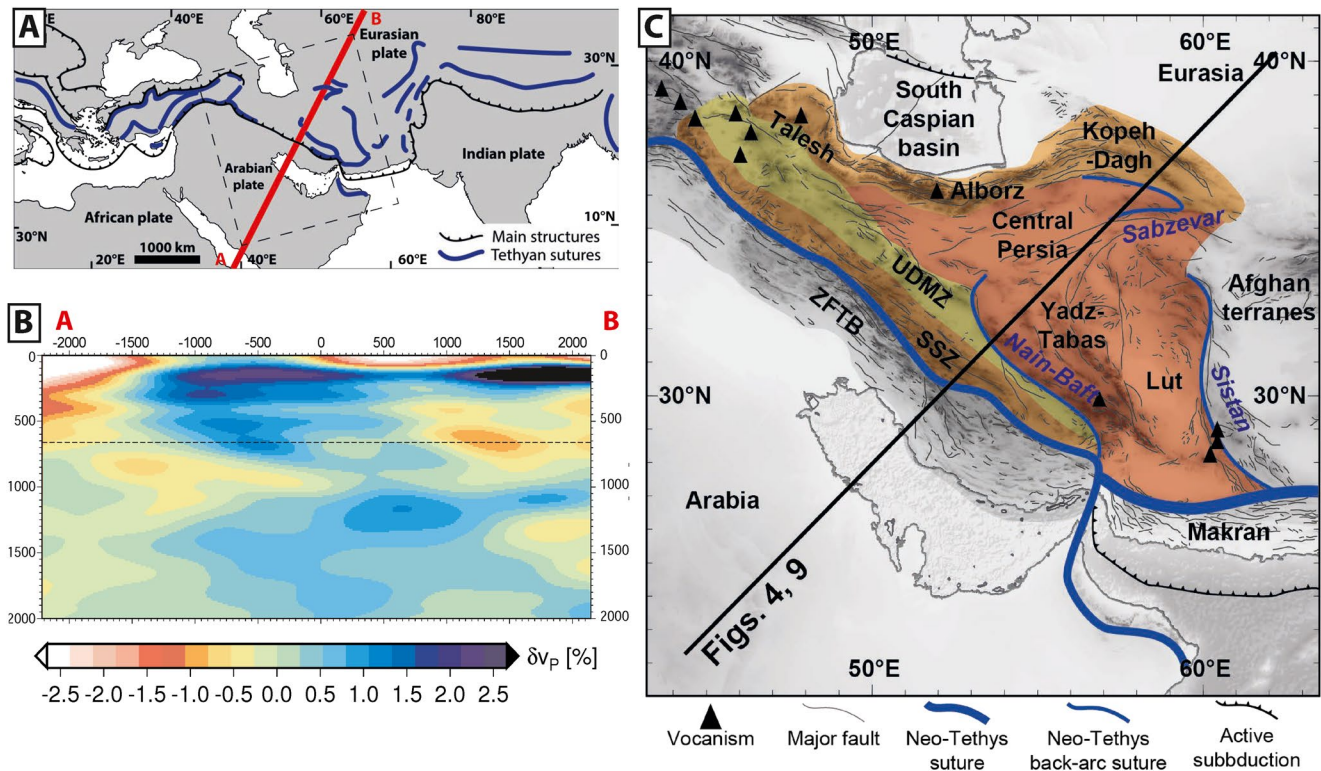


Figure 1. (a) Distribution of the Tethyan realm remnants along the Alpine-Himalayan convergence zone. (b) Tomographic cross-section of the Central Neotethys domain (Obayashi et al., 2013). The Tethyan slab is interpreted as piled up into the lower mantle at $\sim 1,500$ -km depth. (c) Main structural areas of the Western Cimmerian Domain (WCD): the Sanandaj-Sirjan Zone (SSZ), the Urmia-Dokhtar Magmatic Zone (UDMZ), the Talesh-Alborz-Kopeh-Dagh range (TAK), and Central Iran, Yazd-Tabas, and Lut microblocks; and of the main Neotethys sutures and associated back-arcs (i.e., Sabzevar and Nain-Baft). The thick black line represents the trace of the cross-section restored in Figures 4 and 9. ZFTB: Zagros Fold and Thrust Belt.

compressional and extensional episodes associated with magmatic pulses (e.g., Barrier & Vrielynck, 2008; Berberian & Berberian, 1981; Omrani et al., 2008; Rossetti et al., 2010, 2014; Sacconi et al., 2010; Moghadam et al., 2014, 2016, 2020; Tadayon et al., 2017, 2019; Verdel et al., 2011). Each of these pulses of deformation has been so far related to different deep processes, such as slab break-off, flat-slab retreat, or convergence velocity variations (Agard et al., 2011; Rabiee et al., 2020; Tadayon et al., 2019; Verdel et al., 2011). However, a dynamically consistent model able to explain the alternation of compressional and extensional pulses within the upper plate has not yet been proposed.

Here, we relate the upper-plate deformation history of the Iran mobile belt to an unsteady behavior of the slab in the mantle and we explore how slab dynamics may relate to the tectonic regime in the overriding plate. We first review the geological constraints, proposing a new tectonic reconstruction for the area, and we then use 2D numerical modeling to explore the dynamics of the slab in the mantle transition zone (defined hereafter by MTZ). Our results show that we can indeed obtain alternating pulses of back-arc compression and extension using a reasonable range of parameters for the slab-mantle system. If this model is correct, we can then use the Iranian cases as a key area to unravel the behavior of subduction zones over geological time scale.

2. Geological Setting

The Tethyan suture extends along the Alpine-Himalayan convergent front from the Mediterranean area to SE Asia. It developed incrementally during the diachronous closure of various Tethys oceanic realms and branches (Figure 1a). The central part of the Tethyan belt is characterized by two main suture zones, as a consequence of the closure of the Paleo-Tethys and Neotethys oceans. The WCD consists of several crustal blocks (colored areas in Figure 1c), accreted to the Eurasian plate during the late Triassic to early Jurassic

after the consumption of the Paleo-Tethys ocean (e.g., Barrier & Vrielynck, 2008; Berberian & King, 1981; Stampfli & Borel, 2002; Zanchi et al., 2006). After its accretion, the WCD became the southern margin of the Eurasian plate. The opening and the onset of oceanic spreading in the Central Neotethys is Paleozoic in age as documented by marginal sedimentary sequences symmetrically distributed with respect to the Zagros suture and by the occurrence of Triassic to Cretaceous radiolarites covering the Neris and the Kermanshah ophiolites complexes (e.g., Hassanzadeh & Wernicke, 2016; Moghadam & Stern, 2015). The sedimentary cover of the Neotethys ophiolites indicates oceanic conditions free of any significant continental influence during the Mesozoic after the Triassic oceanic break-up of the Neotethys. A second event of oceanic spreading in the Neotethys appears to have occurred during the Cretaceous. Indeed, most of the Neotethys ophiolites indicate that the late Cretaceous oceanic spreading is either MORB-related or associated with a supra-subduction zone (Moghadam & Stern, 2015; Moghadam et al., 2014, 2020). This Cretaceous oceanic spreading occurred most likely shortly before the obduction of the Neotethys ophiolites onto the Arabian margin (e.g., Agard et al., 2011). Eventually, a third Neotethys oceanic spreading event is also proposed for the Eocene (Figure 2; Moghadam & Stern, 2015). The age of the final closure of the Neotethys ocean and the subsequent collision between Arabia and the WCD is still debated but most probably occurred sometime between the late Eocene and the early Oligocene (e.g., Agard et al., 2011; Ballato et al., 2011; Koshnaw et al., 2018; McQuarrie & van Hinsbergen, 2013; Tadayon et al., 2017).

The Western Cimmerian Domain can be divided into four main tectonic subdomains separated by two ophiolitic sutures (Figure 1c). The southern subdomains include the Sanandaj-Sirjan Zone (SSZ) and the Urumia-Dokhtar Magmatic Zone (UDMZ), which represent the Mesozoic and the Cenozoic volcanic arc of the Zagros subduction system, respectively. To the north, the Central Iranian Domain (i.e., Central Iran, Yazd-Tabas, and Lut microblocks) is separated from the SSZ and the Talesh-Alborz-Kopeh-Dagh mountains (TAK) by two ophiolitic zones formed by the suturing of two oceanic back-arc basins (i.e., the southern Nain-Baft and the northern Sabzevar-Sistan, respectively). The TAK mountains constitute the former northern margin of WCD. This margin was first inverted in the early Mesozoic during the closure of the Paleo-Tethys and the collision of the WCD with Eurasia, and then in the late Cenozoic after the closure of the Neotethys and the collision between Eurasia and Arabia (e.g., Barrier & Vrielynck, 2008; Zanchi et al., 2006, 2009).

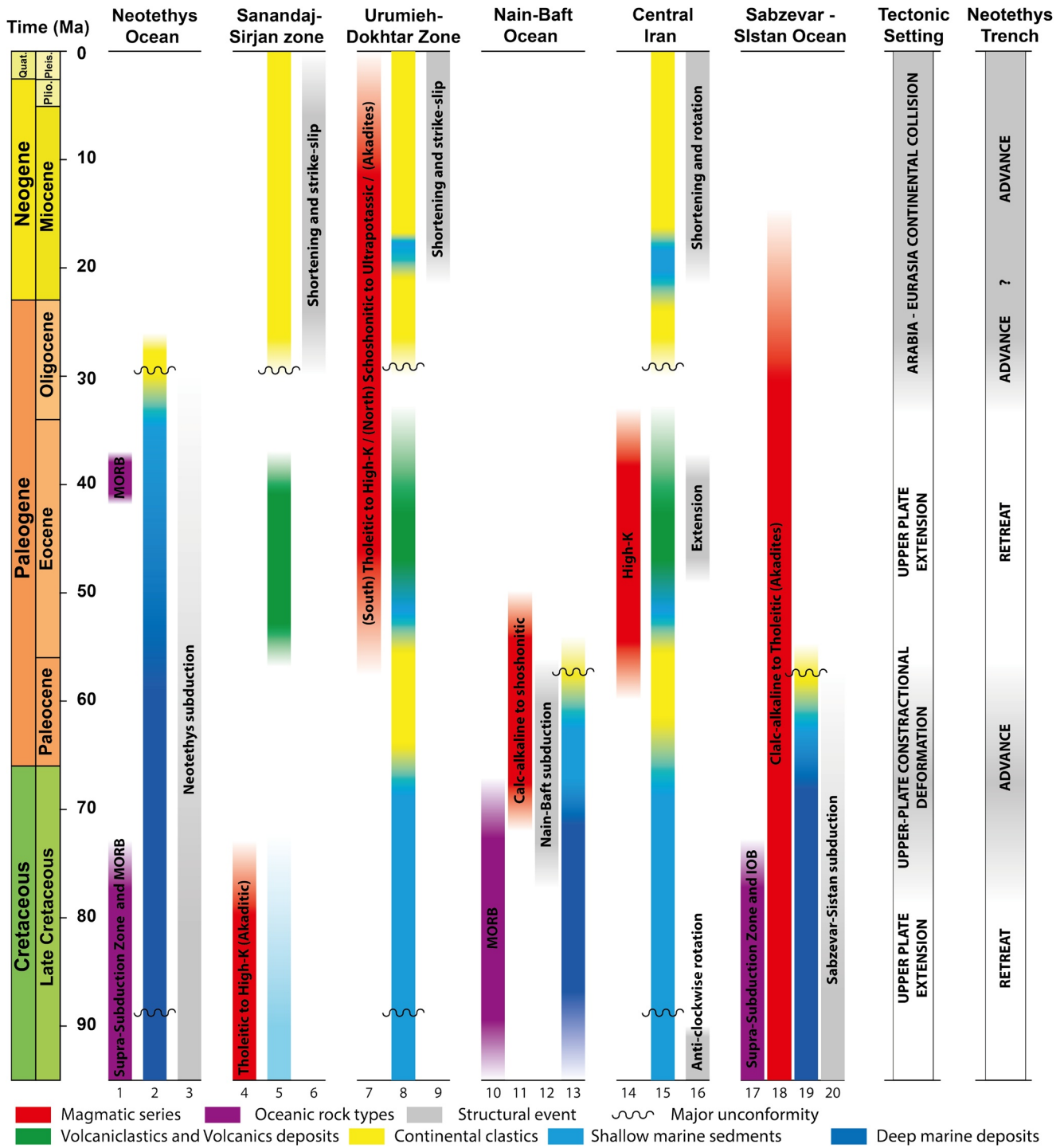
In the following, we provide a brief description of the major tectonic, sedimentary, and magmatic events that characterized each subdomain during the last 100 Ma. These events are compiled in Figure 2.

2.1. The Sanandaj-Sirjan Zone (SSZ)

The SSZ is a 100–150-km wide domain, extending from the Bitlis area in SE Turkey to the Makran accretionary prism in SE Iran (Figure 1c). It is bordered by the main Neotethys suture zone to the SW (i.e., the Bajgan-Durkan complex) and by the UDMZ to the NE. The SSZ is mainly composed of Paleozoic to Upper Cretaceous metamorphic rocks and sedimentary deposits, intruded by Mesozoic igneous rocks with a tholeiitic and calc-alkaline signature (e.g., Omrani et al., 2008). The SSZ has been interpreted as the active margin of the WCD from the middle Jurassic to the Paleogene (e.g., Agard et al., 2011; Hassanzadeh & Wernicke, 2016). Yet, recent isotopic and trace elements signature investigations in some intrusive bodies indicate that the middle-late Jurassic magmatism in the SSZ and the Makran area could be related to continental rifting (Azizi & Stern, 2019; Azizi et al., 2018; Hunziker et al., 2015). This would imply that the onset of the Central Neotethys oceanic subduction did not start earlier than the Cretaceous (Azizi & Stern, 2019; Azizi et al., 2018; Bröcker et al., 2021; Burg, 2018). The SSZ is characterized by a thick lithosphere (up to 225 km), resulting from the underthrusting of the Arabian lithosphere during its collision with the WCD (e.g., Motaghi et al., 2017; Paul et al., 2010; Rahmani et al., 2019).

2.2. Urmia-Dokhtar Magmatic Zone (UDMZ)

The UDMZ is situated between the Central Iranian domain and the SSZ and is partly covering the Nain-Baft ophiolitic belt (Figure 1c). It consists of abundant calc-alkaline and alkaline volcanic rocks of Eocene and to a minor extent Oligo-Miocene to Quaternary ages (e.g., Berberian & King, 1981; Moghadam et al., 2018; Omrani et al., 2008; Rabiee et al., 2020). Early Miocene to Quaternary adakites are found in the northern



and central sectors of the UDMZ (Omrani et al., 2008; Pang et al., 2016). The most recent magmatic activity has occurred in the south-eastern and north-western sectors of the UDMZ and is characterized by alkaline postcollisional lavas (e.g., Jahangiri, 2007). The ~100-km thick lithosphere below the UDMZ (Chen et al., 2016; Priestley et al., 2012) was thinned most likely as the result of partial delamination during the Neogene (Chiu et al., 2013; Neill et al., 2013; Pang et al., 2013).

2.3. Central Iranian Domain

The Central Iranian Domain consists of several lithospheric blocks characterized by a relatively thin and warm lithosphere (Mahmoodabadi et al., 2020). They include the Yazd-Tabas and the Lut blocks, which were separated from each other before the Pan-African orogeny (Figure 1c; e.g., Berberian & King, 1981). After the Precambrian amalgamation, the WCD has been subjected to a complex tectonic history with the reactivation of the blocks boundary faults and the localization of extensional or contractional deformation (e.g., Stöcklin, 1968). The Precambrian to Paleozoic crystalline basement of the Central Iranian Domain is covered by Jurassic to Cretaceous marine deposits, suggesting protracted Mesozoic subsidence (e.g., Wilmsen et al., 2009). A late Cretaceous, Turonian to Coniacian, angular unconformity has been observed in several places of the WCD (e.g., Vaziri et al., 2012; Wilmsen et al., 2015) and in the Kopeh-Dagh area (e.g., Mosavinia & Wilsem, 2011) and has been related to a regional phase of contractional deformation. Widespread subduction-related volcanic activity resumed in the WCD in the earliest Eocene as observed in the UDMZ and in most of the Central Iranian Domain (Verdel et al., 2011).

Importantly, the Central Iranian Domain is West and East bounded by several ophiolitic belts constituting the sutured Neotethys back-arc oceanic domains (e.g., Agard et al., 2011; Moghadam & Stern 2015). The Nain-Baft ophiolitic belt is located in the SW of the Central Iranian domain (Figure 1c) and consists of a series of ophiolitic slices exposed along the Nain-Dehshir and Dehshir-Baft faults (Moghadam et al., 2009). These slices are composed of serpentinitized ultramafic and mafic rocks with MORB signatures (Pirnia et al., 2018) along with radiolarites and limestones indicating a short-lived episode of late Cretaceous oceanic spreading.

The NW-SE striking Sabzevar suture zone extends over a length of ca. 400 km and bounds the Kopeh-Dagh mountains to the north and Central Iran to the south (Figure 1c). Geochemical fingerprints of heterogeneous mantle signatures (MORB dominated) indicate oceanic spreading during late Cretaceous (e.g., Moghadam et al., 2009, 2014; Shojaat et al., 2003). However, early Cretaceous high-pressure granulites found in the Sabzevar ophiolitic suture suggests the existence and the subduction of the Sabzevar ocean earlier than late Cretaceous and a possible connection with the Sistan back-arc ocean (Rossetti et al., 2010). In any case, the Sabzevar oceanic domain subducted below Eurasia during Paleocene times (e.g., Bröcker et al., 2021; Omrani et al., 2013; Rossetti et al., 2014).

The Sistan ophiolitic suture extends roughly N-S over ca. 700 km and separates the Lut block to the W from the Afghan block to the E (Figure 1c). These ophiolites show MORB and supra-subduction zone magmatic signatures and are associated with early to late Cretaceous radiolarites (e.g., Saccani et al., 2010; Zarrinkoub et al., 2012). The subduction of this oceanic domain beneath the Afghan block is thought to have started

Figure 2. Tectono-sedimentary and magmatic chart of the Western Cimmerian Domain (upper plate of the Neotethys subduction system) and associated subdomains according to their structural position from SW to NE (Figure 1). The “Tectonic setting” column summarizes the major upper-plate contractional and extensional phases of deformation. The “Neotethys trench” column synthesis the horizontal motion of the trench accordingly to the deformation episodes affecting the upper plate. Trench advance and retreat periods correspond to upper-plate contraction and extension events, respectively. These episodes of upper-plate deformation and trench horizontal motion are reported in Figure 3. Numbers indicate the references used to build the chart: (1) Aghanabati and Rezaie (2009), Ali et al. (2012), Allahyari et al. (2014), Aswad et al. (2011), Babaie et al. (2006), Ghasemi et al. (2002), Monsef et al. (2010), Saccani et al. (2014), Moghadam and Stern (2015); (2) Agard et al. (2005), Moghadam and Stern (2015); (3) e.g., McQuarrie and van Hinsbergen (2013); (4) e.g., Azizi et al. (2018), Azizi and Jahangiri (2008), Badr et al. (2013), Chiu et al. (2013), Mazhari et al. (2009), Nouri et al. (2016), Omrani et al. (2008), Sepahi and Athari (2006); (5) Falcon (1974); (6) Agard et al. (2005, 2006); (7) Chiu et al. (2013), Omrani et al. (2008); (8) Ballato et al. (2017), Saidi et al. (1997); (9) François et al. (2014); (10) Moghadam et al. (2009), Pirnia et al. (2018); (11) Omrani et al. (2008); (12) Ghazi et al., (2012); (13) Moghadam et al. (2009); (14) Chiu et al. (2017), Verdel et al. (2007); (15) Aghanabati and Rezaie (2009), Allen and Armstrong (2008), Hadi et al. (2019), Saidi et al. (1997), Wilmsen et al. (2005, 2009, 2015, 2018); (16) e.g., Mattei et al. (2015, 2017), Morley et al. (2009), Verdel et al. (2007); (17) Omrani (2008), Moghadam et al. (2014, 2020); (18) Chiu et al. (2013, 2017), Jamshidi et al. (2015); Omrani et al. (2008), Pang et al. (2013, 2014), Rossetti et al. (2014), Moghadam et al. (2014, 2016); (19) Tadayon et al. (2019); (20) Bonnet et al., 2018, Bröcker et al. (2013, 2021), Kurzawa et al. (2017), Rossetti et al. (2010, 2014), Moghadam et al. (2020), Zarrinkoub et al. (2012).

during the late Cretaceous (Bonnet et al., 2018; Bröcker et al., 2013; Kurzawa et al., 2017) and should have lasted until the Paleocene (Saccani et al., 2010).

Finally, it should be noted that in the Central Iranian Domain, from the southern Alborz foothills to the SSZ, Eocene shallow-water marine, nummulite-bearing limestones (Ziarat Formation, ~56-48 My old) rest unconformably over deformed older sedimentary deposits and blueschist units (Macaud erie et al., 1983; Moghadam et al., 2009; Rossetti et al., 2014). These limestones are superseded by Eocene volcanic and volcanoclastics deposits (Karaj Formation) deposited in relatively deep-marine basins (below the photic zone) and evolve up section, virtually everywhere, into latest Eocene shallow-water marine deposits containing nummulites and locally evaporites, and supposed Oligocene red beds of the Lower Red Formation (Davoudzadeh & Weber-Diefenbach, 1997). Similarly, to the Ziarat Formation, upper Oligocene to lower Miocene shallow-water marine limestones of the Qom Formation rest, locally unconformably, over the same area. These deposits appear to be older (late Oligocene) in the proximity of the Neotethys suture and slightly younger (Aquitanian to Burdigalian) in NW Iran and along the southern Alborz mountains (Daneshian & Dana, 2019; Davoudzadeh & Weber-Diefenbach, 1997). In any case, starting from ~17 Ma a continental depositional system was established throughout the WCD as documented by the Upper Red Formation (Ballato et al., 2017). Collectively, these two short-lasting flooding events indicate the occurrence of two regional-scale subsidence episodes that affected the entire southern margin of the Eurasian plate in the latest Paleocene-earliest Eocene and the late Oligocene-early Miocene.

2.4. The Talesh-Alborz-Kopeh-Dagh Mountain Range

The Talesh-Alborz-Kopeh-Dagh mountain range (TAK) forms a sinuous intracontinental orogen sandwiched between the South Caspian Basin and the Central Iranian Domain (Figure 1c). It results from the late Triassic-early Jurassic and late Cenozoic inversion of a stretched continental domain during the closure of the Paleo-Tethys and Neotethys, respectively (e.g., Allen et al., 2003; Axen et al., 2001; Ballato et al., 2015; Guest et al., 2006b, 2007; Lyberis & Manby, 1999; Rezaeian et al., 2012; Robert et al., 2014). In its eastern part (Kopeh-Dagh area), the Paleo-Tethys ophiolitic suture defines the northern boundary of the WCD (Zanchi et al., 2006). The southern flank of the range is characterized by a thickness of several kilometers of Eocene volcanic and volcanoclastics deposits of marine affinity pinching out northward (Ballato et al., 2013; Guest et al., 2006a), while the northern orogenic slope presents coeval, thin (<1 km), shallow-water marine deposits of Caspian affinity. Widespread volcanism in the central Alborz mountains terminated around the latest Eocene (Ballato et al., 2011), while in NW Iran and to the south of the Kopeh-Dagh it has persisted, although punctuated, until the Quaternary (Chiu et al., 2013; Shabanian et al., 2012).

Since the latest Eocene, the TAK has started recording transpressional deformation together with exhumation most likely as a far-field effect of the earliest phases of the Arabia-Eurasia collision (e.g., Allen et al., 2003; Ballato et al., 2011; Guest et al., 2006b, 2007; Lyberis and Manby, 1999; Madanipour et al., 2013; Rezaeian et al., 2012; Robert et al., 2014). Subsequently, from the early-middle Miocene, exhumation rates increased significantly possibly in response to a more advanced stage of the Arabia-Eurasia collision (e.g., Axen et al., 2001; Ballato et al., 2013, 2015; Guest et al., 2006b, 2007; Madanipour et al., 2017; Paknia et al., 2021; Rezaeian et al., 2012). To the north, the South Caspian Basin appears to have started subducting beneath Eurasia at least from the late Miocene (e.g., Mammadov, 2008), possibly when the TAK range started bending around the South Caspian Basin (e.g., Cifelli et al., 2015; Mattei et al., 2017) or following the rapid sediment loading triggered by the ~ 6 to 3 Ma, km-scale (0.6 to 1.4km) base-level fall in the Caspian Sea.

3. Tectonic Reconstruction

Here, we propose a tectonic reconstruction of the Central Iranian domain for the last 100 Ma. During this time interval the subduction of the Neotethys was active and the motion of Eurasia was almost stationary (e.g., Seton et al., 2012). Therefore, the deformation in the plate interior is related to trench migration: the retreat of the trench toward the subducting plate generates upper-plate extension and opening of back-arc basins whereas the advancement of the trench toward the upper plate generates upper-plate compression.

The compilation of structural, stratigraphic, and magmatic data in the WCD documents two episodes of upper-plate extension (from >100 to ~70 Ma and from ~55 to ~35 Ma) alternating with two periods of upper-plate shortening (from ~70 to ~55 Ma and from ~35 Ma to present) (Figure 2). The Cretaceous opening of the Nain-Baft and Sabzevar-Sistan (e.g., Figure 2; Moghadam & Stern, 2015; Moghadam et al., 2009, 2014, 2020; Pirnia et al., 2020; Rossetti et al., 2010, 2014; Verdel et al., 2011; Zarrinkoub et al., 2012) represents the first phase of extension and retreat of the Neotethys trench occurred from >100 to ~75 Ma (Figure 2). The progressive closure of the different back-arcs and their suturing before the middle Eocene (e.g., Rossetti et al., 2014; Moghadam et al., 2009, 2014) suggests the occurrence of a period of upper-plate shortening with the advance of the trench from ~75 to 55 Ma (Figure 2). The widespread Eocene back-arc magmatism and the development of extensional core complexes in Central Iran (e.g., Kargaranbafghi et al., 2012; Moghadam et al., 2016, 2018; Verdel et al., 2011) represent the younger extensional phase associated with trench retreat from ~55 to 35 Ma (Figure 2). Eventually, the late Eocene/early Oligocene continental collision between Arabia and Eurasia has led to significant upper-plate shortening (e.g., Agard et al., 2011), in association with the advance of the Neotethys suture toward the upper plate (Figure 2).

We restore the upper plate and the position of the trench in time using those geological constraints and adopting the following assumptions: (i) Although estimates on the amount of extension and contraction are uncertain we may reasonably assume that the minimum amount of extension necessary to generate back-arc oceanic seafloor spreading is about 150 ± 50 km (Huismans & Beaumont, 2011). The closure of the oceanic basin will then be on the same order. (ii) Though locally relevant, the processes of accretion and erosion at the subduction interface are not considered here. Those processes are thought to be related to shallow processes related to the amount of sediment entering into the trench rather than deep trench dynamics (e.g., Clift & Vannucchi, 2004). (iii) Several paleogeographic reconstructions were proposed in the literature for the Nain-Baft, the Sabzevar, and the Sistan back-arc basins (e.g., Agard et al., 2011; Bagheri & Stampfli, 2008; Barrier & Vrielynck, 2008; Bröcker et al., 2021; Pirnia et al., 2020; Rossetti et al., 2010). These reconstructions include two end-member scenarios: a first one proposing a connection between the Sabzevar and the Sistan oceanic basins, with no connection to the subparallel Nain-Baft basin (Agard et al., 2011; Barrier & Vrielynck, 2008; Rossetti et al., 2010); a second one suggesting a connection between the Nain-Baft and the Sabzevar basins, with no connection to the Sistan basin (e.g., Bagheri & Stampfli, 2008). Following the first hypothesis, here, we propose to connect the Sistan with Sabzevar and to keep the Nain-Baft disconnected from them (Figure 4). In this hypothesis, the opening Sabzevar-Sistan and the Nain-Baft accommodate the middle Cretaceous anticlockwise rotation of Central Iran as proposed by Mattei et al. (2015).

To estimate the amount of plate convergence, we measure the distance between Asia and Arabia along a section perpendicular to the NW-SE subduction zone (Figure 3), using the plate velocity model from Seton et al. (2012). The results are in agreement with previous studies (Agard et al., 2011; McQuarrie & van Hinsbergen, 2013), showing a Late Cretaceous peak in convergence velocity (5–6 cm/yr) followed by a rather constant pattern of convergence rates around 2–3 cm/yr through the Cenozoic (Figure 3). To estimate subduction velocity, we sum up the trench velocity to the convergence velocity for retreating trench and subtract for the case of advancing trench. Figure 3 shows the subduction velocity estimate, revealing an oscillating pattern with a period of 15–20 Myrs (Figure 3). In particular, we observe two periods of relatively lower subduction rates at ~75–55 Ma and ~25–5 Ma and two periods of relatively higher subduction rates in the Cretaceous, until ~75 Ma and at ca. 55–35 Ma (Figure 3).

In the following, we describe in four time steps the main tectonic events during the Neotethys subduction and the final collision between Arabia and Eurasia (Figure 4).

3.1. Cretaceous Neotethys Trench Retreat and Opening of Sabzevar-Sistan and Nain-Baft Back-Arc Basins (Figure 4a)

Magmatic activity in the Sanandaj-Sirjan Zone documents the subduction of the Neotethys ocean from the early Jurassic (e.g., Hassanzadeh & Wernicke, 2016; Omrani et al., 2008), although more recent studies have proposed that subduction initiated in the Cretaceous (Azizi & Stern, 2019; Azizi et al., 2018; Hunziker et al., 2015). In the upper plate, the Nain-Baft oceanic basin opened during the late Cretaceous as documented by MORBs related units (Moghadam et al., 2009; Pirnia et al., 2018). Further to the east, in

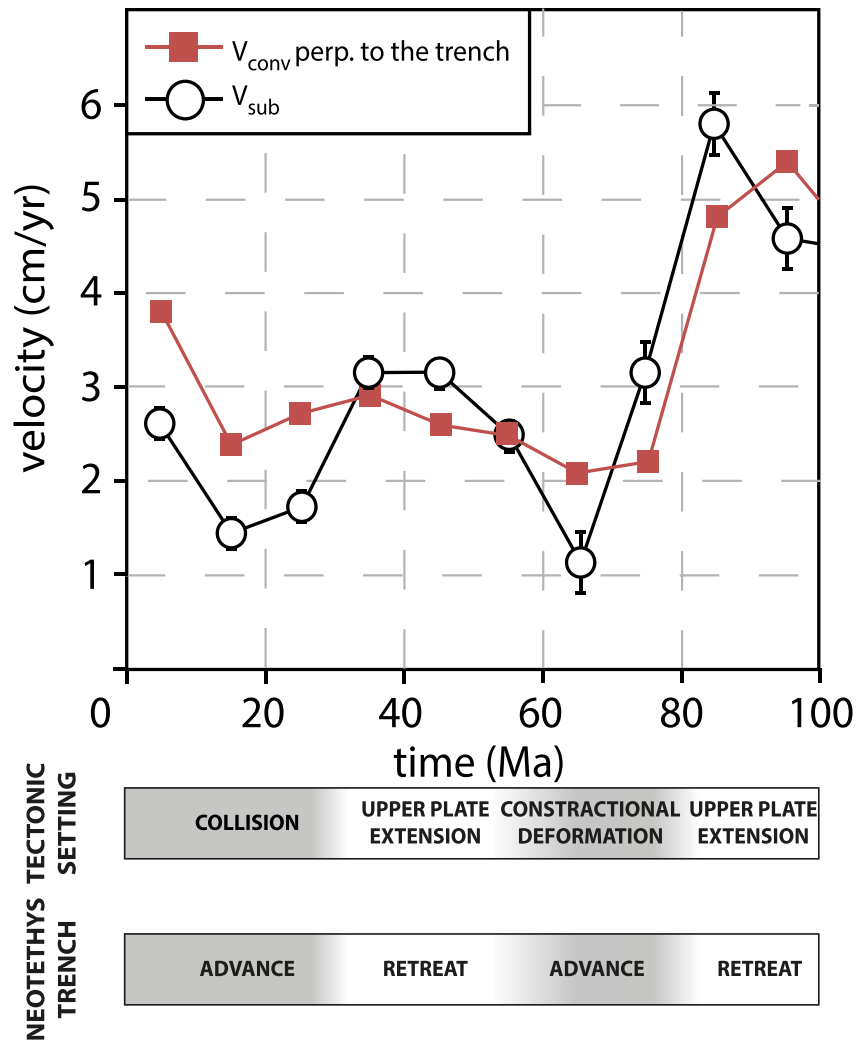
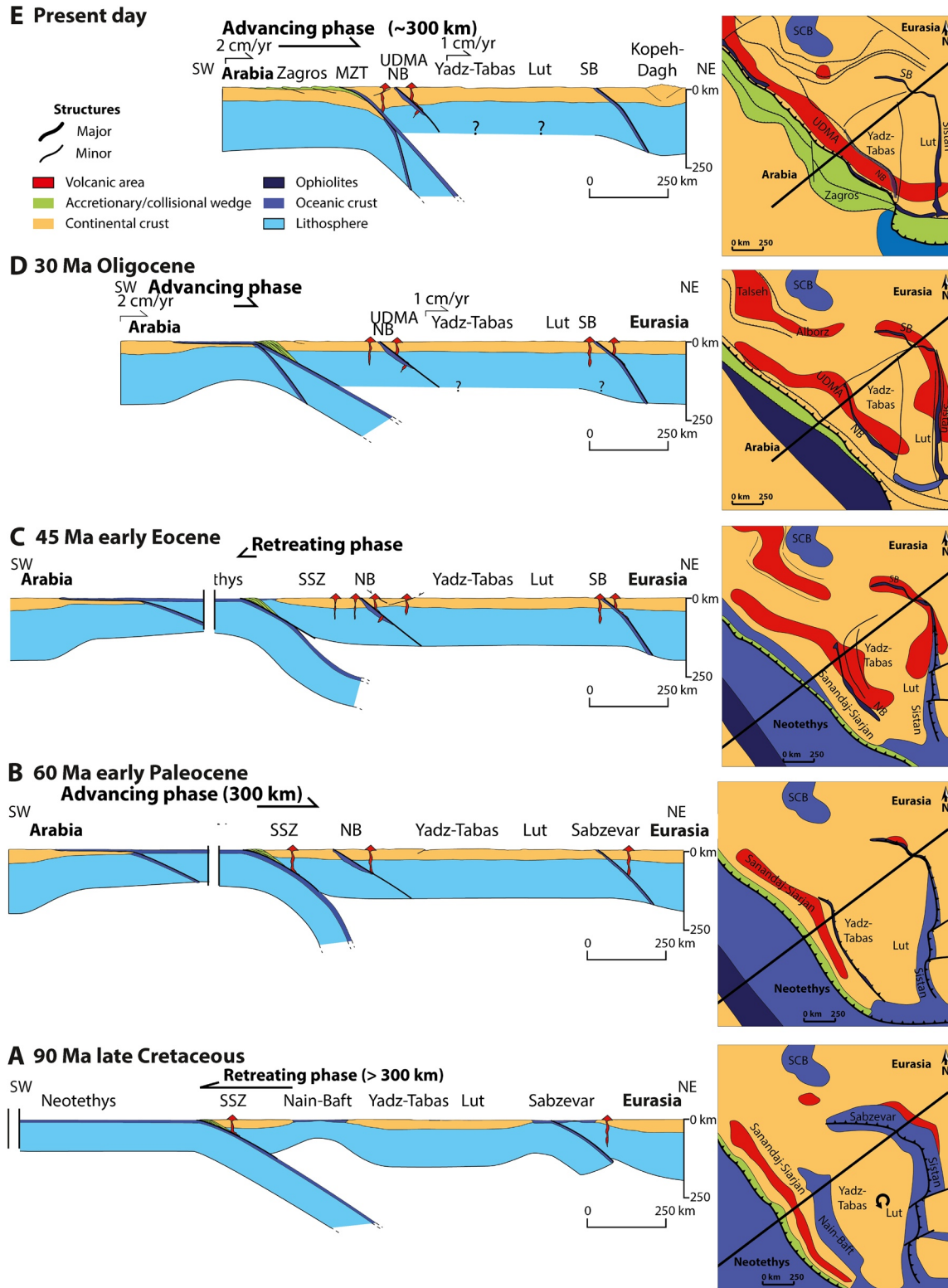


Figure 3. Convergence velocity perpendicular to the trench between two points in Arabia and Eurasia since the early Cretaceous (red square). The velocity model is from Seton et al. (2012). Subduction velocity (white dots) is estimated through the convergence velocity corrected for the trench motion through time (see text). Note that the Late Cretaceous subduction velocity represents a minimum estimate because it does not account for active ocean spreading. We extract the subduction velocity period to confront our models to the Iranian domain evolution (see discussion).

the Sabzevar-Sistan zone, oceanic spreading occurred during the early to late Cretaceous as attested by the presence of MORBs and supra-subduction zone type (Moghadam et al., 2014; Zarrinkoub et al., 2012). Thus, the whole upper-plate domain recorded a significant extension throughout the Cretaceous due to the Neotethys trench retreat (Figure 2). In our reconstruction, we assume a total Neotethys trench retreat of at least 300 ± 100 km for the whole Cretaceous to allow the opening of the Nain-Baft and the Sabzevar-Sistan back-arc basins (Figure 4a). Synchronously, during the early Cretaceous and until 70 Ma, the convergence velocity between Arabia and Eurasia remained high, up to 6 cm/yr until late Cretaceous (Figure 3).

The geochronological age dispersion of ophiolitic units suggests continuous oceanic spreading in the Neotethys from 110 to 73 Ma (Moghadam & Stern, 2015; Moghadam et al., 2020). Geochemical signatures of the Neotethys ophiolites show a transition from MORB to supra-subduction zone along the northern part of the SSZ (Figures 2 and 4a). Thus, during the early Cretaceous, an oceanic ridge formed in the SW part of the Neotethys ocean, allowing the development of MORBs. This ridge was soon inverted leading to the northward intraoceanic subduction of the southern part of the Neotethys followed by the obduction of the central part of the Neotethys above the distal parts of the Arabian plate margin (e.g., Agard et al., 2011).



3.2. Paleocene Neotethys Trench Advance and Closing of the Back-Arc Basins (Figure 4b)

Starting from the late Cretaceous, the Nain-Baft oceanic basin was subducted beneath the Central Iranian Domain until its Paleocene final closure (Moghadam et al., 2009). Similarly, the Sabzevar-Sistan oceanic basin was subducted beneath the Afghan microblocks from the late Cretaceous to the Paleocene (e.g., Bonnet et al., 2018; Bröcker et al., 2013; 2021; Rossetti et al., 2014). The closure of these back-arcs basins indicates an overall upper-plate shortening of about 300 ± 100 km at least, due to the trench advance between the late Cretaceous and the Paleocene (Figure 4b). This shortening episode could have also triggered coeval compressional deformation in the Alborz and Kopeh-Dagh ranges (Ballato et al., 2011; Guest et al., 2006b; Madanipour et al., 2013; Robert et al., 2014) and strike-slip deformation in Central Iran (Tadayon et al., 2017; 2019). It should be noted that, during the upper-plate shortening, between 90 and 70 Ma, the Arabia-Eurasia convergence velocity decreased rapidly to 1–2 cm/yr (Figure 3).

3.3. Early Eocene Northward Arc Migration and Upper-Plate Extension (Figure 4c)

The early to late Eocene time was characterized by a pulse of arc magmatism (Verdel et al., 2011), locally associated with core-complexes, documenting upper-plate extension within the entire Central Iranian Domain (Kargaranbafghi et al., 2012; Moritz et al., 2006; Verdel et al., 2007). This event, together with the northward migration of the volcanic arc from the SSZ to the UDMZ, suggests a decrease in the slab angle (Verdel et al., 2011), a retreat of the trench, and an acceleration of the subduction velocity (Agard et al., 2011). Moreover, in the NW sectors of the Sanandaj-Sirjan Zone, the occurrence of late Eocene supra-subduction type ophiolites (Moghadam & Stern, 2015) suggests a short Neotethys oceanic spreading event, consistent with the upper-plate extension and the trench retreat regime. Considering that in the Central Iranian Domain, Eocene oceanic spreading has not been recorded we assume a Neotethys trench retreat and associated upper-plate extension of maximum 100 ± 50 km (Figure 4c).

3.4. Arabia-Eurasia Collision (Figure 4d)

The onset of the Arabia-Eurasia collision is considered to have occurred sometime between the late Eocene (e.g., Agard et al., 2011; Ballato et al., 2011; Barber et al., 2018; Tadayon et al., 2019) and the early Miocene (e.g., Berberian & Berberian, 1981; Mouthereau, 2011), although recent studies documented that the collision must have occurred not later than the early Oligocene (e.g., Koshnaw et al., 2018; McQuarrie & van Hinsbergen, 2013; Pirouz et al., 2017). Between 30–35 and ~20 Ma collisional deformation was very limited, while the subduction velocity decreased to 1.5–2.0 cm/yr (Figure 3). Shortening increased across the entire collision zone by 20 Ma leading to the accretion of the Arabian passive margin to the upper plate with the formation of the High Zagros mountains (e.g., Barber et al., 2018; Mouthereau, 2011), and the gradual development of a 50–60-km thick crust (Figure 4a, e.g., Paul et al., 2006). At the same time, the Zagros Fold and Thrust Belt experienced a progressive outward (orogen perpendicular) expansion (e.g., Pirouz et al., 2015). Overall, we estimate ~300 km of upper-plate shortening: $\sim 75 \pm 10$ km for the South Caspian Basin subduction amount (Green et al., 2009; Mouthereau, 2011), $\sim 50 \pm 10$ km in the Alborz (Guest et al., 2006a), $\sim 50 \pm 10$ km in the NE Central Iran (Morley et al., 2009), $\sim 60 \pm 20$ km in the suture zone, and $\sim 130 \pm 30$ km for the Sanandaj-Sirjan Zone and the suture zone (Agard et al., 2006; Mouthereau, 2011) due to advancing trench motion (Figure 4a).

In the upper plate, collisional deformation triggered shortening, exhumation, and thrusting of the Sanandaj-Sirjan Zone onto the Neotethys ophiolites starting from the early Oligocene (Barber et al., 2018;

Figure 4. Schematic cross-sections and associated paleotectonic maps for the central Neotethys domain. (a) Early to late Cretaceous, ante 90 Ma stage. The Neotethys trench is largely retreating (at least 300 km) leading to Nain-Baft and Sabzevar-Sistan back-arc opening. (b) Early Paleocene, ~60 Ma. The Neotethys trench advance (~180 km) triggers subduction and closure of the Nain-Baft and Sabzevar-Sistan back-arc basin, in association with widespread shortening in the entire overriding plate. (c) Early Eocene (45 Ma). The Neotethys trench retreat (~50 km) drives extension and core complex formation in Central Iran. The Neotethys fore-arc basin develops in a supra-subduction zone setting, to the SW of the Eurasian margin in the present-day setting of the SSZ. (d and e) Present-day and Oligocene (30 Ma) reconstructions showing the northward motion of the Neotethys suture resulting in shortening in the Sanandaj-Sirjan Zone, Central Iran and Kopeh-Dagh, in association with the northward migration of the volcanic arc (Urumia-Dokthar Magmatic Zone). Arabia Present-day crustal thickness is after Gvirtzman et al. (2016); NB: Nain-Baft back-arc basin; UDMZ: Urumia-Dokthar Magmatic Zone; SCB: South Caspian Basin; SSZ: Sanandaj-Sirjan Zone.

François et al., 2014). The initial stages of collisional deformation affected also the Talesh-Alborz area, with diffuse Oligocene basin inversion followed by a diachronous acceleration in shortening and exhumation rates from the early-middle Miocene to the Pliocene (e.g., Ballato et al., 2011, 2015; Guest et al., 2006a; Madanipour et al., 2013, 2017; Paknia et al., 2021; Rezaeian et al., 2012).

In the early to middle Miocene, an extensional or transtensional deformation phase occurred in the Central Iranian Domain (Morley et al., 2009). This event was associated with the deposition of the shallow-water marine limestones of the Qom Formation (and possibly the base of the superseding Upper Red Formation). Coevally, we observed the acceleration of exhumation in the SSZ (François et al., 2014) and the increase in the Arabia-Eurasia convergence velocity (Figure 3).

Eventually, since the late Miocene, the collisional deformation triggered a major reorganization of the Central Iran area (e.g., Calzolari et al., 2016; Jentzer et al., 2017; Nozaem et al., 2013; Tadayon et al., 2017), the oroclinal bending of the Talesh-Alborz and Kopeh-Dagh around the South Caspian Basin (SCB) (Cifelli et al., 2015; Mattei et al., 2017), and the subduction of the SCB beneath the Absheron Ridge with the development of an accretionary prism (Allen et al., 2002; Axen et al., 2001; Ballato et al., 2015; Jackson et al., 2002; Mammadov, 2008).

Summing up, the occurrence of late Cretaceous to early Paleogene opening and closing of back-arc basins and the Eocene extensional event followed by the latest Eocene to early Oligocene collisional deformation indicates that the upper-plate experienced at least two major episodes of extension and compression. The episode of extension is also accompanied by diffuse magmatism and subsidence (Figure 2). Several processes have been proposed to explain this evolution. For example, the early Tertiary extensional episode has been related to slab roll-back, following an episode of flat subduction, analogous to Laramide evolution in the western US (Verdel et al., 2011) or slab break-off (Agard et al., 2011). Here, we propose an alternative model, where episodes of compression and extension are produced by trench advance and retreat episodes, respectively. We also suggest that trench oscillation from retreating to advancing, is due to repeated episodes of slab folding phase in the mantle transition zone (e.g., Guillaume et al., 2009; Ribe et al., 2007). In the following, we will first present a simple numerical model of slab folding and after we will discuss how this may explain the phases of deformation observed in the Iran mobile belt.

4. Numerical Model

4.1. Model Setup

We use a thermo-compositional 2D numerical model of single-sided subduction to investigate how trench advance and retreat episodes may be reproduced during subduction. The model is not specifically designed to simulate the case of the Central Neotethys but rather to explore an emergent behavior of possible slab deformation during its accumulation into the mantle transition zone and deeper penetration into the lower mantle. The models have been selected from a parametric modeling study showing the surface response to deep subduction (Briaud et al., 2020).

The model is performed using the finite element code CITCOM (Agrusta et al., 2017; Moresi & Gurnis, 1996; Wang et al., 2015; Zhong & Gurnis, 1994) to solve the governing equations in an incompressible (Boussinesq approximation) viscous fluid with negligible inertia and zero internal heating. The setup is constituted by a Cartesian box with a depth of 3,000 km corresponding to the whole mantle depth. The aspect ratio of depth versus width of the model is 1:3. A mobile mid-ocean ridge is positioned on the subducting plate, and another oceanic ridge is positioned on the trailing edge of the upper plate (Figure 5a). Hence, the upper plate is free to move relative to the side of the box. All boundaries are considered impermeable (i.e., free slip boundaries). As a result, the mantle is restricted to the size of the domain, and its motion is driven by the internal buoyancy forces. The rectangular nonuniform mesh is defined by $2,880 \times 472$ elements where the finest elements size of 2.5 km^2 is localized in the trench region.

The model described here is set with the following parameters (see also Briaud et al., 2020). The thermal initial condition is set at 2,773 K at the core-mantle boundary and 273 K on the surface. The upper plate is continental, with a constant initial thermal thickness of 100 km, and is composed of a 30 km crust with a density of $2,700 \text{ kg/m}^3$ whereas the underlying lithosphere has a density of $3,300 \text{ kg/m}^3$. The subducting

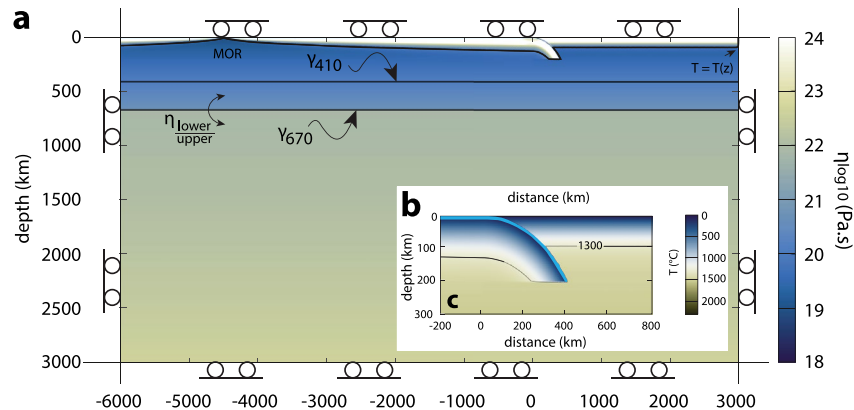


Figure 5. (a) Sketch of the model domain at $t = 0$ Ma of a subducting lithosphere with an initial plate age of 100 Ma. The light blue layer at the top of the subducting plate represents the weak viscosity layer of 10^{20} Pa s (oceanic crust) that decouples the subduction system. The background colors are scaled to the viscosity field, while the two horizontal black lines (γ_{410} ; γ_{670}) represent the equilibrium position of the phase boundaries of olivine-wadsleyite at 410 km and the postspinel transition at 670 km. Two oceanic ridges (MOR) of the subducting plate and the upper plate are also indicated. Little rollers on the box sides correspond to the free slip boundary conditions. (b) Zoom in on the subduction system. Background color corresponds to the initial temperature conditions. The Thick-blue layer represents the weak layer that decouples the plates. The black solid line represents the 1,300 °C isotherm.

plate is oceanic and its thickness is defined by the half-space cooling. On top of the subducting lithosphere, a 7.5-km thick low viscosity layer (1×10^{20} Pa s, Figure 5b) is presented down to 200-km depth to facilitate subduction and plate decoupling. The subduction is initiated by prescribing an asymmetric geometry in the trench region, which provides the initial instability required for free subduction (Figure 5b).

The reference viscosity used in this study is 10^{20} Pa s. The average viscosity of the upper mantle (0–670-km depth) is set to be at about 10^{20} Pa s and the average lower mantle (670–3,000 km) viscosity is set between 10^{21} and 5×10^{22} Pa s. Two olivine phase transitions (γ , Clapeyron slope) are assumed at (1) 410 km (olivine-wadsleyite; γ_{410}) and (2) 670 km (ringwoodite-postspinel; γ_{670}) depths. The density increases for a mantle composed of wt. 100% of olivine associated with phase changes are (1) $\Delta\rho_{410} = 250 \text{ kg/m}^3$ and (2) $\Delta\rho_{670} = 350 \text{ kg/m}^3$ for γ_{410} and γ_{670} , respectively. The γ_{410} phase transition strength locally increases the pull of the slab. By contrast, the combination of viscosity increases with depth, and γ_{670} may inhibit the flow between upper and lower mantle. Previous studies documented changes in the slab morphology that influence the mantle convective pattern over a wide range of plausible values for the two-phase transitions (γ_{410} ; γ_{670}) and the mantle viscosity contrast (Agrusta et al., 2017; Briaud et al., 2020; Christensen, 1996; Čížková & Bina, 2013; Garel et al., 2014; Kincaid & Olson, 1987; Mao & Zhong, 2018).

The model shown here aims to specifically illustrate the surface response to deep slab deformation. For this, we run a series of models testing: i) the influence of the 410-km olivine to wadsleyite (γ_{410}) and the 670-km wadsleyite-ringwoodite to postspinel (γ_{670}) phase transitions, ii) the viscosity contrast, iii) the slab buoyancy and iv) the strength (modulated by slab age) of the slab at the transition zone. As for the phase change, we explore a wide reasonable range of values (e.g., Agrusta et al., 2017; Cizkova et al., 2012) assuming the mantle composed of wt. 100% olivine.

4.2. Results

Figure 6a illustrates a snapshot of four model run, representative of four styles or categories of slab-lower mantle interaction for different phase transition strengths and upper/lower mantle viscosity jumps. Figure 6a shows a case without phase transition and viscosity jump, where the slab readily enters within the lower mantle at a high angle (Category 1). Imposing a weak exothermic phase transition ($\gamma_{410} < +3.5$ MPa/K), a relatively strong endothermic phase at 670-km depth ($\gamma_{670} < -2$ MPa/K) and a viscosity jump, instead, results in slab stagnation laying down into the mantle transition zone (Figure 6, Category 2). Increasing also the (ol-wd) 410 km phase transition ($\gamma_{410} > +3.5$ MPa/K) produces slab folding at the transition zone with slow lower mantle penetration (Figure 6c, Category 3). Imposing also a stronger endothermic phase at

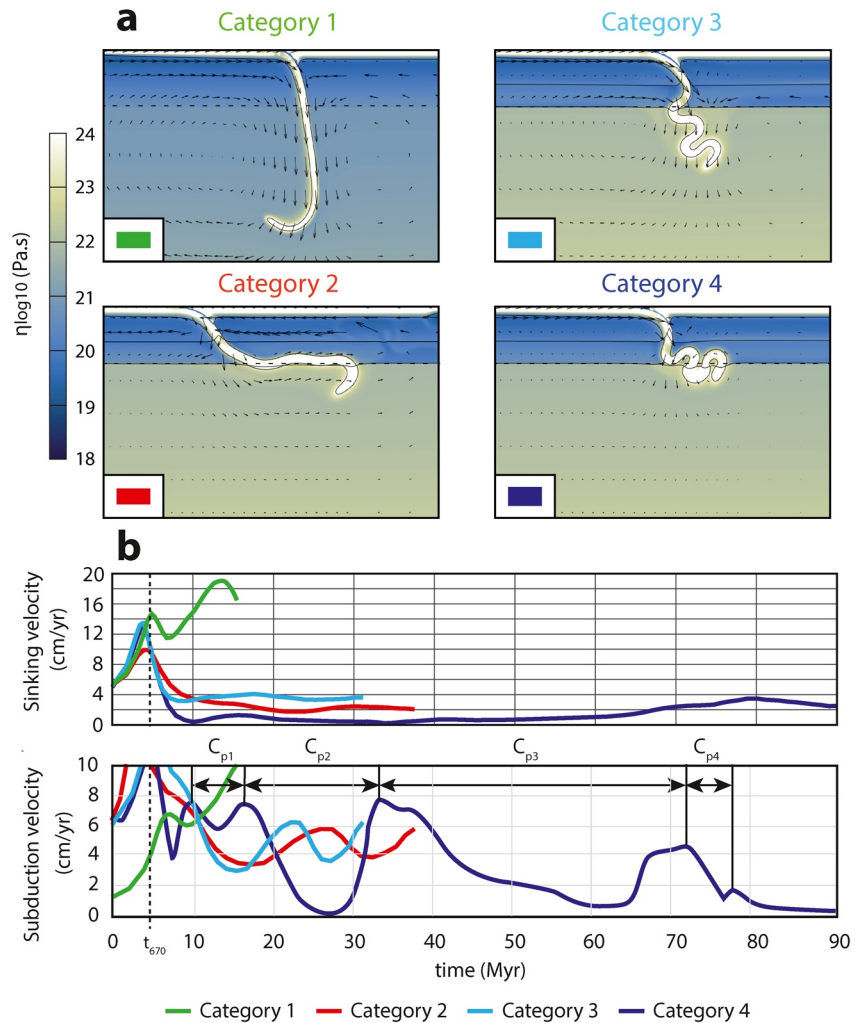


Figure 6. (a) Snapshots of four slab-MTZ categories, as defined in Briaud et al. (2020). (b) Time series of sinking slab velocity (V_s) and subduction velocity period (S_p) for the four cases in (a): (Category 1) undisturbed slab; (Category 2), flat slab; (Category 3) folding slab; (Category 4) buckling slab and avalanche. Subduction velocity period: $S_p = \sum_{i=1}^n S_p(n)$. MTZ, mantle transition zone.

670-km depth ($\gamma_{670} < -2.8$ MPa/K) would trap slab into the MTZ while folding, followed by an episode of slab avalanche into the lower mantle (Category 4).

Figure 7 illustrates in detail the evolution of a Category 4 model, showing surface topography (top panels) and the horizontal component of the stress tensor (hereafter, σ_{xx}). Figure 8 also shows average topography (far from plate edges), trench migration, velocity, and slab dip change through time. The topography here includes both the isostatic topographic signal, due to crustal deformation, and the dynamic topographic signal, due to mantle convection.

In the initial phase, the slab sinks subvertically into the upper mantle (Figures 7a and 8e), producing an increase in subduction velocities (Figures 8c and 8d), compression (>40 MPa) close to the trench, and upper-plate extension of ~ 5 km at a distance of $>1,000$ km from the trench. Once the slab reaches the transition zone, it starts folding (Figure 7b) producing a decrease in subduction velocity (Figures 8c and 8d) while the upper plate shows uplift and extension (Figures 8a and 8b).

From 6 to 60 Myr (Figures 7b–7d), the slab folds back and frontward in the transition zone, changing its dip (Figure 8e) and its subduction velocity (Figure 8d). These variations in velocity correspond to periods of trenches advance and retreat (Figure 8c), topography uplift and subsidence, and horizontal stress evolutions

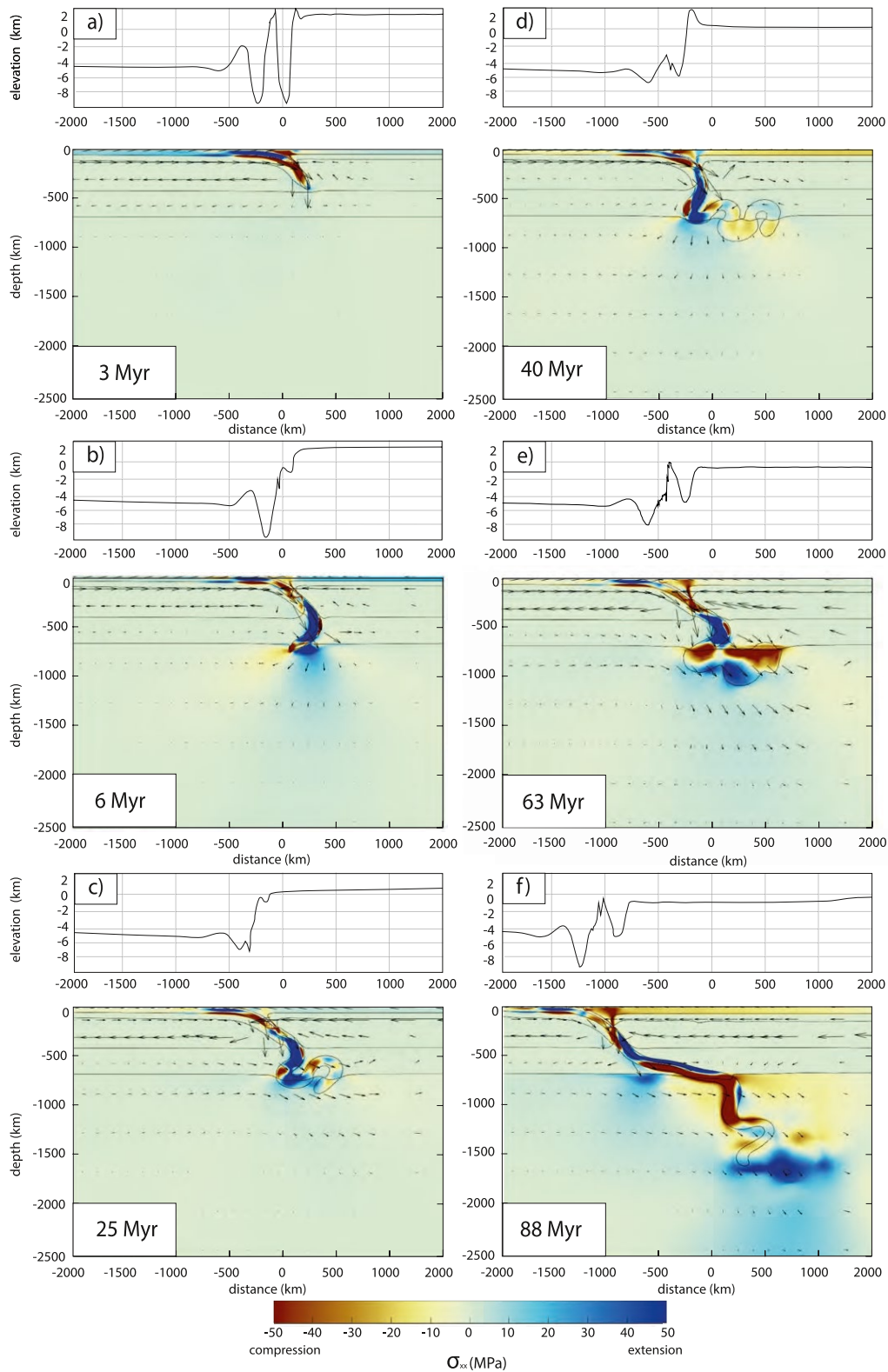


Figure 7. Evolution of a subduction model of slab folding and avalanching at different time steps. The upper panels show the surface topography, while the lower panel shows the horizontal component of the stress tensor (σ_{xx}). Overlain on the stress field plots of the model, the velocity vectors, and the slab contours are also represented (1,300 °C isotherm). The mantle transition zone is localized between the two black lines at 410-km and 670-km depth, respectively.

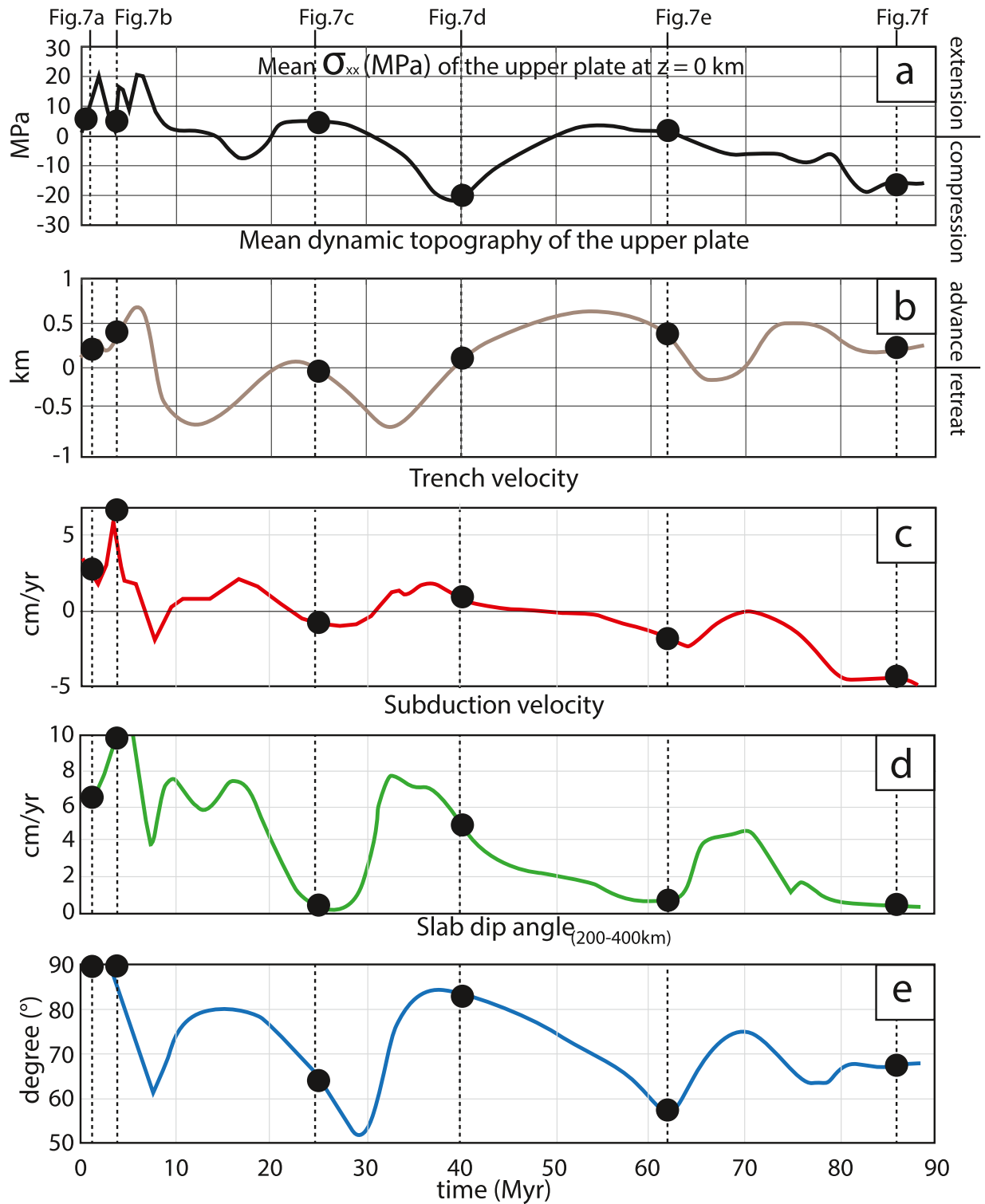


Figure 8. Kinematics and geometry features of the model in time. Dashed lines indicate the time steps shown in Figure 7. Horizontal stress σ_{xx} and the dynamic topography are averaged from the central part of the upper plate between 800 and 2,200 km to avoid side effects. The slab dip angle is measured between 100 and 400 km of depth.

from compression to extension within the upper plate (Figures 8a and 8b). This upper-plate deformation follows the trench and subduction velocities peaks in time with a delay for the dynamic topography of about 5 Myr. In detail, slab bending toward the upper plate produces slab steepening, trench advance (Figure 7d), topography growth, and upper-plate compression (Figures 7a and 7b). It induces also, a return flow cells of a small radius localized in the wedge side of the subduction zone (Figure 6d). In contrast, slab folding backward induces slab shallowing, trench retreats (Figure 6c), upper-plate subsidence with an overall tilting toward the trench (Figures 7c and 7e), and upper plate extension (Figure 7b). This slab dynamic and morphology produces strongly asymmetric mantle flow, with large-scale return flow focused on the wedge side of the slab (Figure 6c).

Around 60 Myr (Figure 7e) the slab starts flushing down into the lower mantle. During this event, subduction velocity increases and the upper-plate subsides while getting in compression. After a few Myrs (~10–15), the evolutionary pattern changes again, and the subduction velocity decreases while the slab advances with a gradual compression of the upper plate toward the trench (Figure 7a).

4.3. Interpretation

The 2D numerical models provide insights into the slab dynamics in the mantle transition zone and its effect on the stress state and the topographic evolution of the overriding plate. The model confirms previous findings (e.g., Agrusta et al., 2017; Christensen, 1996; Čížková et al., 2007; Cramer et al., 2017; Guillou-Frotier et al., 1995; Houseman & Gubbins, 1997; Zhong & Gurnis, 1994) and shows that slab thickening and folding in the MTZ are favored by an increase in the lower mantle viscosity and a relatively high Clapeyron slopes strength, which in turn produce increased resistance to slab penetration into the lower mantle. When the slab folds and piles up into the transition zone, we observe episodic changes in the state of stress as well as in the topographic evolution of the upper plate (Figures 7 and 8). In particular, extension and subsidence are observed when slab folds backward inducing slab roll-back. In contrast, large-scale compression and uplift are observed when the slab folds and roll-over toward the upper plate (Figures 7d and 8). Furthermore, our models show that the flushing into the lower mantle results in subsidence and compression followed by slab shallowing, trench retreat, and a decrease in subduction velocities (Cramer et al., 2017; Faccenna et al., 2017). These observations can be directly compared and used to interpret variations in the state of deformation of the upper plate.

Figure 9 summarizes these observations illustrating the model behavior with respect to the period of the subduction velocity (S_p), the averaged time between peaks of the subduction velocity time series, and the averages sinking velocity of the slab in the mantle (V_s). The representation of our modeling results in this parameter space, allow differentiating the four categories shown in Figure 6b.

Category 1 shows no periodicity for S_p over the high rates of sinking slab velocity as imposed by the strength of the Clapeyron slopes, the slab strength, and the weak viscosity contrast between the upper and lower mantle. Category 2 clusters around relatively slow sinking velocities (<1.3 cm/yr) as slabs did not penetrate into the lower mantle with S_p values ranging between 9.5 and 38 Myr. This category shows that the viscosity contrast increases with S_p while an increase in the slab strength does not change S_p drastically. Category 3 represents slabs that fold and penetrate directly into the lower mantle. This category shows a wide range of V_s due to the strength of both Clapeyron slopes (γ_{410} ; γ_{670}) while the S_p is similar to the previous Category 2. This suggests that periods of compression are mostly controlled by periods of slab folding into the transition zone. Finally, Category 4 is characterized by slab folding and avalanche. This category shows higher S_p values (starting from 20 Myr) and V_s rates ranging from 0.9 to 2.2 cm/yr. The variation in S_p is primarily linked to the ability of the slab to sink into the lower mantle. Indeed, high lower mantle viscosity induces a higher period in the subduction velocity. It means that the slab is trapped for a long time in the MTZ. By contrast, lower viscosity contrast between the upper and lower mantle induces a shorter period in the subduction velocity. The strength of the slab for Category 4 shows that both old ($A_{\text{plate}} = 150$ Myr) and young slab ($A_{\text{plate}} = 25$ Myr) induce a shorter time period of S_p . Our study suggests that the strongest factors governing the slab folding period are the viscosity contrast between the upper and lower mantle and the strength of the slab (Figure 9). A possible application to a specific case such as the Iranian mobile belt will be discussed in the following section.

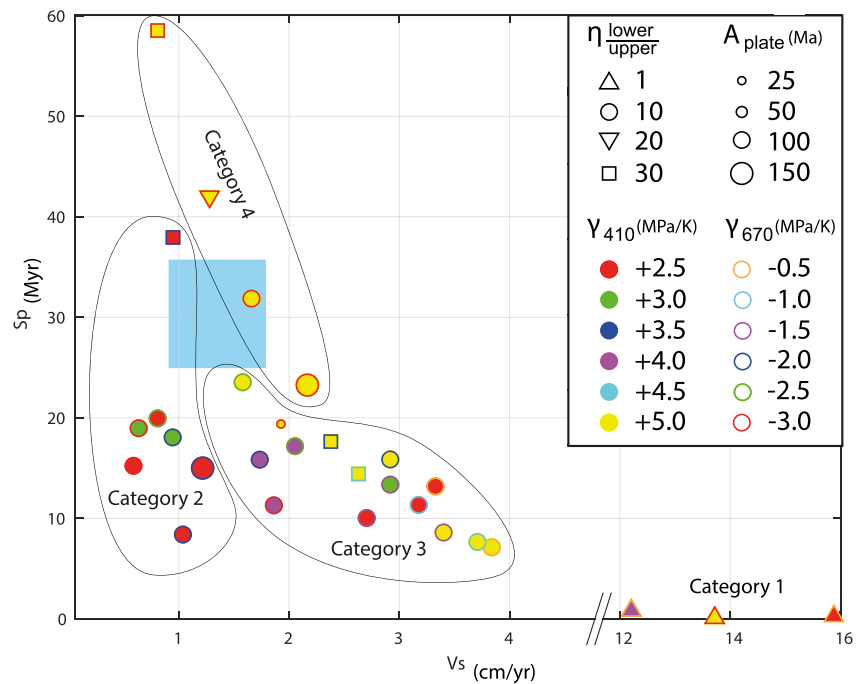


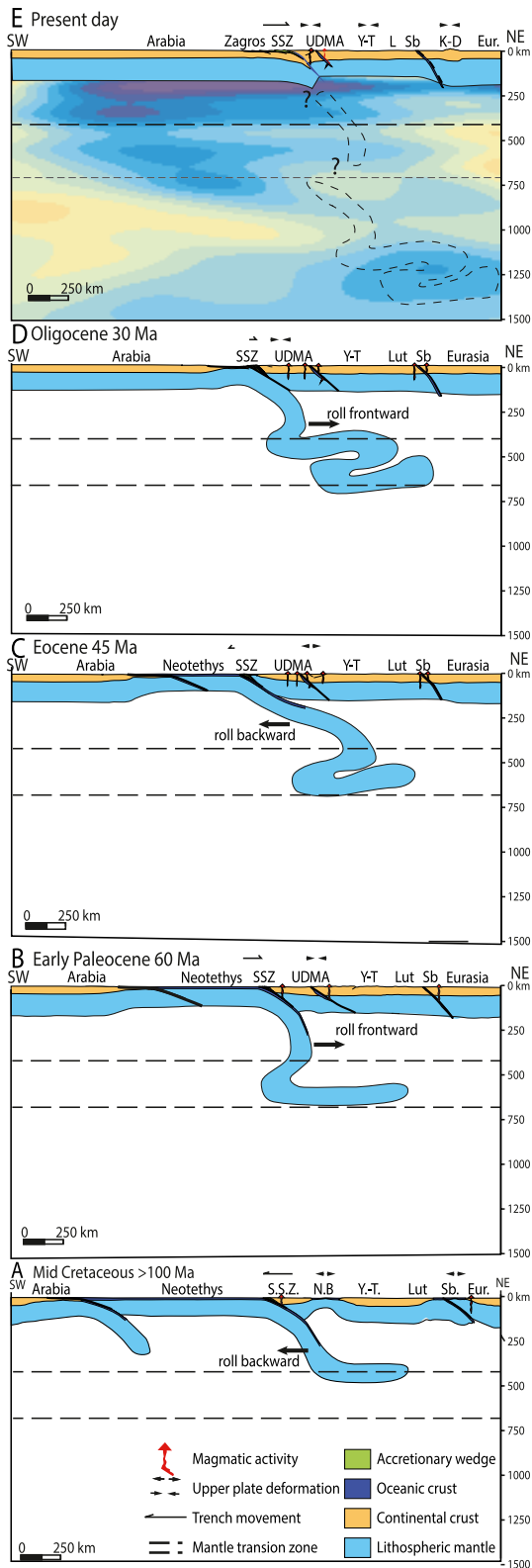
Figure 9. Diagram showing the result of the numerical model as a function of S_p , which represents the averaged time between peaks of the subduction velocity, and V_s , which represents the average sinking slab velocity. The colors of the dots indicate the strength of the Clapeyron slopes whereas their shapes are the mantle viscosity contrast as mentioned in Briaud et al., (2020). The blue area corresponds to the plausible location of the Central Neotethys slab inferred as inferred by tectonic reconstruction (Figure 4) and tomographic images.

5. Discussion

The deformation history of the Iran mobile belt is characterized by distinctive episodes of contraction and extension that occurred in the interior of the upper plate, far from the plate boundary. Specifically, we recognized two episodes of back-arc extension, from 100 and 80 Ma and from 40 to 60 Ma, and two episodes of compression, from 70 to 55 Ma and from 35 Ma to present. The last one is induced by the arrival of the Arabian continental plate at the trench. These episodes are interpreted here to represent periods of retreating and advancing trench, that produced large-scale extension and compression, respectively.

Several models have been proposed to explain every single episode of tectonic deformation. In particular, trench retreat has been invoked for the Eocene extension and magmatism, following a period of flat subduction associated with the late Cretaceous to Paleocene contractional deformation (Verdel et al., 2011). This model, however, does not explain why extension and magmatism occurred during subsidence and marine flooding. Previous studies proposed also the presence of two or three episodes of slab break-off of the Central Tethyan subduction zone based on geological signals and tomography images. For example, Agard et al. (2011) proposed a slab break-off at 60-40 Ma. The 60-40 Ma back-arc extensional event is supposed to have induced a major shift in arc magmatism and to have triggered widespread extension within the upper plate. Slab break-off, however, is expected to produce uplift and a decrease in the subduction velocity due to a drop in the slab pull level. Again, the presence of a middle Eocene marine flooding associated with large-scale subsidence, and the increase in the subduction velocity from 65 Ma onward (Figures 2 and 3), is not in agreement with the Paleogene slab break-off interpretation.

The hypothesis of slab break-off is supported by tomographic images showing the presence of a deep high-velocity anomaly at 1,200–2,000 km, within the lower mantle, and possibly separated from a shallower one (Figures 1 and S1). Van der Meer et al. (2018) interpreted this deep high-velocity anomaly as an old slab break-off episode and hence as an anomaly disconnected from the upper mantle one. However, such dis-



connection can likely occur during the slab penetration in the lower mantle as demonstrated by recent numerical simulation (i.e., slab orphaning event, Grima et al., 2020).

Several models suggest a more recent (Late Miocene) and shallow slab break-off or partial tear of the slab (e.g., Agard et al., 2011). We consider this recent slab deformation episode well-suited in the frame of a continental collision marking the end of a long subduction history.

Here, we propose for the first time in the region, another possible solution that explains the episodic and alternating deformation pattern observed in the Iranian mobile belt. Such a solution is backed up by the results of our physical modeling, guiding our interpretation of the subduction history in the Central Neotethys area. The periodicity of the subduction velocity (Figure 3) and with the maximum slab depth inferred from tomographic images (e.g., Agard et al., 2011; Lu & Grand, 2016; Obayashi et al., 2013; Ritsema et al., 2011; Van der Meer et al., 2018; Van der Voo et al., 2000) can be well explained by slab folding at the MTZ followed by penetration into the lower mantle (Figure 8).

Considering the Neotethys subduction onset during the middle Cretaceous (i.e., 110–130 Ma; e.g., Azizi & Stern, 2019; Burg, 2018) and a maximum slab depth at 1,200–2,000 km (Figures 1b and S1; Agard et al., 2011; Auer et al., 2014; Lu & Grand, 2016; Obayashi et al., 2013; Ritsema et al., 2011; Van der Meer et al., 2018; Van der Voo et al., 2000), we can estimate for the Neotethys slab a sinking velocity in the mantle of about 0.9–1.8 cm/yr. Moreover, considering a temporal time frame between an extensional and a compressional episode of about 25–35 Myrs, we can imagine that the Neotethys subduction system is in the range of the parameters of the blue rectangle of Figure 9. We may then relate the Neotethys upper-plate episodic deformation and its topographic evolution over the last 90 Ma to the behavior of the slab at depth (Figure 10), in a similar way to the model of Categories 3 and 4 of Figure 9. It is interesting to note that similar temporal behaviour have been also described for the Cordillera system and related to cycle of eclogite root development and subsequent foundering (De Celles et al., 2009). The model proposed here may then represent an alternative deep mantle solution that could be valid also for the Farallon-Nazca subduction system (Guillaume et al., 2009; Ribe et al., 2007).

In our reconstruction, the slab reaches the mantle transition zone before 100 Ma leading to the trench retreat and upper-plate extension (Figures 2 and 10a). The opening of the Sabzevar-Sistan back-arc ocean started during the early Cretaceous and was driven by the Neotethys trench retreat during high Arabia-Eurasia convergence velocity (Figures 3 and 4a). For such a high convergence velocity (about 6 cm/yr for 30–40 Ma), the total amount of subducted Neotethys should correspond to 1,800–2,400 km. Yet note that the convergence between Arabia and Eurasia during the middle Cretaceous is accommodated by both the Neotethys subduction zone beneath the Iranian domain and the intraoceanic subduction which led to the ophiolite emplacement above the Arabian margin (e.g., Agard et al., 2007). Thus, the total length of Neotethys ocean subducted during the middle Cretaceous should be split into the intraoceanic subduction and beneath the Iranian Domain (Figure 10a). The Neotethys trench retreat and the upper-plate extension lasted until the Late Cretaceous as attested by the oceanic spreading of the Nain-Baft and Sabzevar back-arc basins (e.g., Moghadam et al., 2009, 2014; Pirnia et al., 2020). Slab roll-back induced widespread upper-plate subsidence in association with regional flooding as documented by the occurrence of deep-marine Cretaceous deposits in the Central Iran Domain (e.g., Wilmsen et al., 2015).

We propose that, from the early to the late Cretaceous, the Neotethys slab flattened at the mantle transition zone, leading to trench retreat, back-arc extension, and subsidence of the upper plate (Figure 10b). The following closure and inversion of the Nain-Baft

and the northern part of the Sabzevar-Sistan oceanic basins during Paleocene indicate a switch of the tectonic regime (Figure 2). This event is also attested by the activation of dextral intraplate strike-slip tectonics in Central Iran (Tadayon et al., 2019). We associate the Paleocene compression to the Neotethys trench advance (Figure 3) that could be explained by a frontward folding of the slab in the mantle transition zone (Figure 10b).

During the Eocene, the magmatic pulse recorded along the entire WCD produced a large amount of continental-arc magmatism (Verdel et al., 2011). A coeval episode of upper-plate extension is found in the Central Iran Domain area, as shown by the occurrence of metamorphic complexes between the Yazd and Tabas microblocks (Kargaranbafghi et al., 2012). Besides, the deposition of late Paleocene to Eocene shallow-water marine limestones from the Sistan to the UDMZ and the TAK suggests widespread, almost synchronous, upper-plate subsidence (Hadi et al., 2019). According to our reconstruction, the Neotethys trench retreated during this period leading to upper-plate extension and the development of Neotethys oceanic supra-subduction type ophiolites in the northern SSZ (Moghadam & Stern, 2015). We, therefore, propose that subsidence of the WCD and associated magmatism and extension is due to the backward folding of the Neotethys slab into the MTZ and its consequent slab roll-back and trench retreat (Figures 2 and 10c). The intense magmatic event during this phase can be then correlated with a speed-up of subduction velocity inducing intense return flow-related decompression melting (e.g., Agard et al., 2011; Faccenna et al., 2010).

The continental collision, started during the latest Eocene-earliest Oligocene, producing both lower and upper-plate shortening (Tadayon et al., 2017), crustal accretion (Mouthereau, 2011), the relative advance of the former Neotethys trench (i.e., the suture zone) of about ~150 km (Figures 10d and 10e), and the decrease in the convergence velocity (Figure 3). During the collision, we register a possible increase of the convergence velocity since 15 Ma and a short episode (probably lasting <5 My) of widespread upper-plate subsidence as attested by the deposition of upper Oligocene to lower Miocene shallow-water marine limestones of the Qom Formation (Figure 2). Such a large-scale subsidence episode during crustal shortening and thickening cannot be interpreted in terms of isostasy. Here, we likely relate this peculiar subsidence event to the penetration of the Neotethys slab into the lower mantle inducing the dynamical subsidence of the upper plate (Figure 10e), as already described in other regions along the Tethyan slab (Yang et al., 2016, 2018). Note that, our numerical models do not include the collision of the upper plate with a continental lithosphere and therefore the general finding interpreted from them could differ from the Neogene tectonic history observed in the Iranian domain. Yet, we consider the evolution of the Neotethys subduction as a possible natural analogue of the models of Category 4 of Figure 9. In these models, the slab penetration into the lower mantle after piling-up in the MTZ produces a large-scale tilting of the upper plate toward the trench (Figure 7e) while the subduction velocity increases (Figure 8d).

6. Conclusions

In this study, we design a set of numerical models to explain the impact of slab folding into the mantle transition zone (MTZ), on the mode of upper-plate deformation and its topographic evolution. This slab behavior is mainly a consequence of the Clapeyron slope strength and in a minor contribution of the mantle viscosity contrast and the slab strength. The main results of the numerical models are then applied to the Neotethys subduction system in the Iranian domain. This allows proposing a new evolutionary model that can explain the periodicity of upper-plate deformation with the slab behavior at depth. The main points for the Neotethys subduction zone can be summarized as follows:

1. The opening of the Nain-Baft, Sabzevar, and Sitan back-arc basins is related to the Neotethys slab roll-back and trench retreat during the middle Cretaceous, possibly when the slab anchored at the MTZ
2. The closures of the back-arc basins during the late Cretaceous and the Paleocene are linked to the Neotethys slab folding at the MTZ due to trench advance toward the upper plate

Figure 10. Interpreted tomographic section (panel E from Obayashi et al., 2013) and reconstruction of the Central Neotethys subduction system along a SW-NE section (Panel A to D). The interpretation of the tomographic section pattern (panel E) includes the possibility of recent and shallow slab break off episode (e.g., Agard et al., 2011) and deep slab disconnection (orphaning, Grima et al., 2020). The pre-collisional history (panel A to D) illustrates slab folding episodes and the upper plate episodic deformation (see text for discussion). Uninterpreted tomographic section and location is on Figure 1 and Figure S1. NB: Nain-Baft; Sb: Sabzevar; SSZ: Sanandaj-Sirjan Zone; UDMZ: Urumia-Dokhtar Magmatic Zone; Y-T: Yazd-Tabas microblock.

3. The Eocene stretching of the Iranian domain and associated back-arc magmatism and subsidence is related to a new phase of slab folding, roll-back, and trench retreat
4. After the late Eocene/early Oligocene onset of the Arabia-Eurasia collision, the Neotethys suture continues advancing toward the Iranian Domain
5. The middle Miocene subsidence and flooding of the Iranian Domain may be interpreted as a consequence of the sinking of the pillowed Neotethys slab into the lower mantle

Overall, our results show that the tectonic history of the upper plate of the Neotethys subduction system can be explained by slab folding at the MTZ and its subsequent sinking into the lower mantle.

Data Availability Statement

Results of the numerical modeling are available at <https://doi.org/10.5281/zenodo.3824437>.

Acknowledgments

The authors would like to thank the editor L. Jolivet and M. Gurnis, E. Shabanian, and B. Wernicke for their constructive comments and criticisms which allowed us to greatly improve our work, and Thorsten Becker for comments and to provide Figure S1. This work has been supported by: (i) Prin2017-2020 (Geodynamics of the Arabia-Eurasia collisional zones, PI C. Faccenna), (ii) Equinor project Temadyn; (iii) MIUR (Ministry of Education University and Research), Excellence Department Initiative granted to the Department of Science, University of Roma Tre, (Art. 1, com. 314-337, Low 232/2016). P. Ballato was supported by the MIUR (Ministry of Education University and Research), with a Rita Levi Montalchini grant. The supporting information contains four tomographic cross-sections of the studied area.

References

- Agard, P., Jolivet, L., Vrielynck, B., Burov, E., & Monié, P. (2007). Plate acceleration: The obduction trigger? *Earth and Planetary Science Letters*, 258(3–4), 428–441. <https://doi.org/10.1016/j.epsl.2007.04.002>
- Agard, P., Monié, P., Gerber, W., Omrani, J., Molinaro, M., Meyer, B., et al. (2006). Transient, synobduction exhumation of Zagros blueschists inferred from P-T, deformation, time, and kinematic constraints: Implications for Neotethyan wedge dynamics. *Journal of Geophysical Research*, 111, B11401. <https://doi.org/10.1029/2005JB004103>
- Agard, P., Omrani, J., Jolivet, L., & Mouthereau, F. (2005). Convergence history across Zagros (Iran): Constraints from collisional and earlier deformation. *International Journal of Earth Sciences (Geol Rundsch)*, 94, 401–419. <https://doi.org/10.1007/s00531-005-0481-4>
- Agard, P., Omrani, J., Jolivet, L., Whitechurch, H., Vrielynck, B., Spakman, W., et al. (2011). Zagros orogeny: A subduction-dominated process. *Geological Magazine*, 148(5–6), 692–725. <https://doi.org/10.1017/S001675681100046X>
- Aghanabati, A., & Rezaie, A. (2009). *Correlation of lithostratigraphic units of Iran in major structural and sedimentary basins*.
- Agrusta, R., Goes, S., & van Hunen, J. (2017). Subducting-slab transition-zone interaction: Stagnation, penetration and mode switches. *Earth and Planetary Science Letters*, 464, 10–23. <https://doi.org/10.1016/j.epsl.2017.02.005>
- Ali, S. A., Buckman, S., Aswad, K. J., Jones, B. G., Ismail, S. A., & Nutman, A. P. (2012). Recognition of late cretaceous Hasanbag ophiolite-arc rocks in the Kurdistan region of the Iraqi Zagros suture zone: A missing link in the paleogeography of the closing Neotethys Ocean. *Lithosphere*, 4(5), 395–410. <https://doi.org/10.1130/L1207.1>
- Allahyari, K., Saccani, E., Rahimzadeh, B., & Zeda, O. (2014). Mineral chemistry and petrology of highly magnesian ultramafic cumulates from the Sarve-Abad (Sawlava) ophiolites (Kurdistan, NW Iran): New evidence for boninitic magmatism in intra-oceanic fore-arc setting in the Neo-Tethys between Arabia and Iran. *Journal of Asian Earth Sciences*, 79, 312–328. <https://doi.org/10.1016/j.jseas.2013.10.005>
- Allen, M. B., & Armstrong, H. A. (2008). Arabia-Eurasia collision and the forcing of mid-Cenozoic global cooling. *Palaeogeography, Palaeoclimatology, Palaeoecology*, 265(1–2), 52–58. <https://doi.org/10.1016/j.palaeo.2008.04.021>
- Allen, M. B., Ghassemi, M. R., Shahrabi, M., & Qorashi, M. (2003). Accommodation of late Cenozoic oblique shortening in the Alborz range, northern Iran. *Journal of Structural Geology*, 25(5), 659–672. [https://doi.org/10.1016/S0191-8141\(02\)00064-0](https://doi.org/10.1016/S0191-8141(02)00064-0)
- Allen, M. B., Jones, S., Ismail-Zadeh, A., Simmons, M., & Anderson, L. (2002). Onset of subduction as the cause of rapid Pliocene-Quaternary subsidence in the South Caspian basin. *Geology*, 30(9), 775–778. [https://doi.org/10.1130/0091-7613\(2002\)030<0775:OOSATC>2.0.CO;2](https://doi.org/10.1130/0091-7613(2002)030<0775:OOSATC>2.0.CO;2)
- Aswad, K. J. A., Aziz, N. R. H., & Koyi, H. A. (2011). Cr-spinel compositions in serpentinites and their implications for the petro-tectonic history of the Zagros Suture Zone, Kurdistan Region, Iraq. *Geological Magazine*, 148(5–6), 802–818. <https://doi.org/10.1017/S0016756811000422>
- Auer, L., Boschi, L., Becker, T. W., Nissen-Meyer, T., & Giardini, D. (2014). Savani: A variable resolution whole-mantle model of anisotropic shear velocity variations based on multiple data sets. *Journal of Geophysical Research: Solid Earth*, 119, 3006–3034. <https://doi.org/10.1002/2013JB010773>
- Axen, G. J., Lam, P. S., Grove, M., Stockli, D. F., & Hassanzadeh, J. (2001). Exhumation of the west-central Alborz Mountains, Iran, Caspian subsidence, and collision-related tectonics. *Geology*, 29(6), 559–562. [https://doi.org/10.1130/0091-7613\(2001\)029<0559:EOTWCA>2.0.CO;2](https://doi.org/10.1130/0091-7613(2001)029<0559:EOTWCA>2.0.CO;2)
- Azizi, H., & Jahangiri, A. (2008). Cretaceous subduction-related volcanism in the northern Sanandaj-Sirjan Zone, Iran. *Journal of Geodynamics*, 45(4–5), 178–190. <https://doi.org/10.1016/j.jog.2007.11.001>
- Azizi, H., Lucci, F., Stern, R. J., Hasannejad, S., & Asahara, Y. (2018). The Late Jurassic Panjeh submarine volcano in the northern Sanandaj-Sirjan Zone, northwest Iran: Mantle plume or active margin? *Lithos*, 308–309, 364–380. <https://doi.org/10.1016/j.lithos.2018.03.019>
- Azizi, H., & Stern, R. J. (2019). Jurassic igneous rocks of the central Sanandaj-Sirjan zone (Iran) mark a propagating continental rift, not a magmatic arc. *Terra Nova*, 31(5), 415–423. <https://doi.org/10.1111/ter.12404>
- Babaei, H. A., Babaei, A., Ghazi, A. M., & Arvin, M. (2006). Geochemical, ⁴⁰Ar/³⁹Ar age, and isotopic data for crustal rocks of the Neyriz ophiolite, Iran. *Canadian Journal of Earth Sciences*, 43(1), 57–70. <https://doi.org/10.1139/e05-111>
- Badr, M. J., Collins, A. S., & Masoudi, F. (2013). The U-Pb age, geochemistry and tectonic significance of granitoids in the Soursat complex, Northwest Iran. *Turkish Journal of Earth Sciences*, 22(1), 1–31.
- Bagheri, S., & Stampfli, G. M. (2008). The Anarak, Jandaq and Posht-e-Badam metamorphic complexes in central Iran: New geological data, relationships and tectonic implications. *Tectonophysics*, 451(1–4), 123–155. <https://doi.org/10.1016/j.tecto.2007.11.047>
- Ballato, P., Cifelli, F., Heidarzadeh, G., Ghassemi, M. R., Wickert, A. D., Hassanzadeh, J., et al. (2017). Tectono-sedimentary evolution of the northern Iranian Plateau: Insights from middle-late Miocene foreland-basin deposits. *Basin Research*, 29(4), 417–446. <https://doi.org/10.1111/bre.12180>
- Ballato, P., Landgraf, A., Schildgen, T. F., Stockli, D. F., Fox, M., Ghassemi, M. R., et al. (2015). The growth of a mountain belt forced by base-level fall: Tectonics and surface processes during the evolution of the Alborz Mountains, N Iran. *Earth and Planetary Science Letters*, 425, 204–218. <https://doi.org/10.1016/j.epsl.2015.05.051>

- Ballato, P., Stockli, D. F., Ghassemi, M. R., Landgraf, A., Strecker, M. R., Hassanzadeh, J., et al. (2013). Accommodation of transpressional strain in the Arabia-Eurasia collision zone: New constraints from (U-Th)/He thermochronology in the Alborz mountains, north Iran. *Tectonics*, 32, 1–18. <https://doi.org/10.1029/2012TC003159>
- Ballato, P., Uba, C. E., Landgraf, A., Strecker, M. R., Sudo, M., Stockli, D. F., et al. (2011). Arabia-Eurasia continental collision: Insights from late Tertiary foreland-basin evolution in the Alborz Mountains, Northern Iran. *Geological Society of America Bulletin*, 123(1–2), 106–131. <https://doi.org/10.1130/B30091.1>
- Barber, D. E., Stockli, D. F., Horton, B. K., & Koshnaw, R. I. (2018). Cenozoic exhumation and foreland basin evolution of the zagros orogen during the Arabia-Eurasia collision, Western Iran. *Tectonics*, 37, 4396–4420. <https://doi.org/10.1029/2018TC005328>
- Barrier, É., & Vrielynck, B. (2008). *Palaeotectonic map of the Middle East, Atlas of 14 maps, tectonosedimentary-palinspastic maps from Late Norian to Pliocene*. Paris, France: Commission for the Geologic Map of the World (CCMW, CCGM).
- Berberian, F., & Berberian, M. (1981). Tectono-plutonic episodes in Iran. *Zagros Hindu Kush Himalaya Geodynamic Evolution*, 3, 5–32. <https://doi.org/10.1029/gd003p0005>
- Berberian, M., & King, G. C. P. (1981). Towards a paleogeography and tectonic evolution of Iran. *Canadian Journal of Earth Sciences*, 18(2), 210–265. <https://doi.org/10.1139/e81-019>
- Bonnet, G., Agard, P., Angiboust, S., Monié, P., Jentzer, M., Omrani, J. et al., (2018). Tectonic slicing and mixing processes along the subduction interface: The Sistan example (Eastern Iran). *Lithos*, 310–311, 269–287. <https://doi.org/10.1016/j.lithos.2018.04.016>
- Briaud, A., Agrusta, R., Faccenna, C., Funicello, F., & Hunen, J. (2020). Topographic fingerprint of deep mantle subduction. *Journal of Geophysical Research: Solid Earth*, 125, e2019JB017962. <https://doi.org/10.1029/2019JB017962>
- Bröcker, M., Fotoohi Rad, G., Burgess, R., Theunissen, S., Paderin, I., Rodionov, N., & Salimi, Z. (2013). New age constraints for the geodynamic evolution of the Sistan Suture Zone, eastern Iran. *Lithos*, 170–171, 17–34. <https://doi.org/10.1016/j.lithos.2013.02.012>
- Bröcker, M., Omrani, H., Berndt, J., & Moslempour, M. E. (2021). Unravelling metamorphic ages of suture zone rocks from the Sabzevar and Makran areas (Iran): Robust age constraints for the larger Arabia–Eurasian collision zone. *Journal of Metamorphic Geology*. <https://doi.org/10.1111/jmg.12603>
- Burg, J.-P. (2018). Geology of the onshore Makran accretionary wedge: Synthesis and tectonic interpretation. *Earth-Science Reviews*, 185, 1210–1231. <https://doi.org/10.1016/j.earscirev.2018.09.011>
- Calzolari, G., Della Seta, M., Rossetti, F., Nozaem, R., Vignaroli, G., Cosentino, D., & Faccenna, C. (2016). Geomorphic signal of active faulting at the northern edge of Lut Block: Insights on the kinematic scenario of Central Iran. *Tectonics*, 35, 76–102. <https://doi.org/10.1002/2015TC003869>
- Cerpa, N. G., Araya, R., Gerbault, M., & Hassani, R. (2015). Relationship between slab dip and topography segmentation in an oblique subduction zone: Insights from numerical modeling. *Geophysical Research Letters*, 42, 5786–5795. <https://doi.org/10.1002/2015GL064047>
- Chen, L., Jiang, M., Talebian, M., Ghods, A., Chung, S.-L., Ai, Y., et al. (2016). *New seismic array observation in the Northwestern Iranian Plateau*, EGUGA. EPSC2016-3427.
- Chiu, H.-Y., Chung, S.-L., Zarrinkoub, M. H., Melkonyan, R., Pang, K.-N., Lee, H.-Y., et al. (2017). Zircon Hf isotopic constraints on magmatic and tectonic evolution in Iran: Implications for crustal growth in the Tethyan orogenic belt. *Journal of Asian Earth Sciences*, 145, 652–669. <https://doi.org/10.1016/j.jseae.2017.06.011>
- Chiu, H.-Y., Chung, S.-L., Zarrinkoub, M. H., Mohammadi, S. S., Khatib, M. M., & Iizuka, Y. (2013). Zircon U-Pb age constraints from Iran on the magmatic evolution related to Neotethyan subduction and Zagros orogeny. *Lithos*, 162–163, 70–87. <https://doi.org/10.1016/j.lithos.2013.01.006>
- Christensen, U. R. (1996). The influence of trench migration on slab penetration into the lower mantle. *Earth and Planetary Science Letters*, 140, 27–39. [https://doi.org/10.1016/0012-821x\(96\)00023-4](https://doi.org/10.1016/0012-821x(96)00023-4)
- Cifelli, F., Ballato, P., Alimohammadian, H., Sabouri, J., & Mattei, M. (2015). Tectonic magnetic lineation and oroclinal bending of the Alborz range: Implications on the Southern Caspian Geodynamics. *Tectonics*, 34, 116–132. <https://doi.org/10.1002/2014TC003626>
- Čížková, H., & Bina, C. R. (2013). Effects of mantle and subduction-interface rheologies on slab stagnation and trench rollback. *Earth and Planetary Science Letters*, 379, 95–103
- Čížková, H., van den Berg, A. P., Spakman, W., & Matyska, C. (2012). The viscosity of Earth's lower mantle inferred from sinking speed of subducted lithosphere. *Physics of the Earth and Planetary Interiors*, 200–201, 56–62. <https://doi.org/10.1016/j.pepi.2012.02.010>
- Čížková, H., van Hunen, J., & van den Berg, A. (2007). Stress distribution within subducting slabs and their deformation in the transition zone. *Physics of the Earth and Planetary Interiors*, 161(3–4), 202–214.
- Clark, S. R., Stegman, D., & Müller, R. D. (2008). Episodicity in back-arc tectonic regimes. *Physics of the Earth and Planetary Interiors*, 171, 265–279. <https://doi.org/10.1016/j.pepi.2008.04.012>
- Clift, P., & Vannucchi, P. (2004). Controls on tectonic accretion versus erosion in subduction zones: Implications for the origin and recycling of the continental crust. *Reviews of Geophysics*, 42, RG2001. <https://doi.org/10.1029/2003RG000127>
- Cramer, F., Lithgow-Bertelloni, C. R., & Tackley, P. J. (2017). The dynamical control of subduction parameters on surface topography. *Geochemistry, Geophysics, Geosystems*, 18, 1661–1687. <https://doi.org/10.1002/2017GC00821>
- Daneshian, J., & Dana, L. R. (2019). Benthic foraminiferal events of the Qom Formation in the north Central Iran zone. *Paleontological Research*, 23(1), 10–22. <https://doi.org/10.2517/2018pr008>
- Dávila, F. M., & Lithgow-Bertelloni, C. (2015). Dynamic uplift during slab flattening. *Earth and Planetary Science Letters*, 425, 34–43. <https://doi.org/10.1016/j.epsl.2015.05.026>
- Davoudzadeh, M., & Weber-Diefenbach, K. (1997). Paleogeography, stratigraphy, and tectonics of the tertiary of Iran. *Neues Jahrbuch für Geologie und Paläontologie-Abhandlungen*, 205, 33–67. <https://doi.org/10.1127/njgpa/205/1997/33>
- DeCelles, P. G., Ducea, M. N., Kapp, P., & Zandt, G. (2009). Cyclicity in Cordilleran orogenic systems. *Nature Geoscience*, 2(4), 251–257. <https://doi.org/10.1038/ngeo469>
- Faccenna, C., Becker, T. W., Lallemand, S., Lagabrielle, Y., Funicello, F., & Piromallo, C. (2010). Subduction-triggered magmatic pulses: A new class of plumes? *Earth and Planetary Science Letters*, 299(1–2), 54–68. <https://doi.org/10.1016/j.epsl.2010.08.012>
- Faccenna, C., Becker, T. W., Lucente, F. P., Jolivet, L., & Rossetti, F. (2001). History of subduction and back-arc extension in the central Mediterranean. *Geophysical Journal International*, 145(3), 809–820. <https://doi.org/10.1046/j.0959-540X.2001.01435.x>
- Faccenna, C., Oncken, O., Holt, A. F., & Becker, T. W. (2017). Initiation of the Andean orogeny by lower mantle subduction. *Earth and Planetary Science Letters*, 463, 189–201. <https://doi.org/10.1016/j.epsl.2017.01.041>
- Falcon, N. L. (1974). Southern Iran: Zagros Mountains. *Geological Society Special Publication*, 4, 199–211. <https://doi.org/10.1144/GSL.SP.2005.004.01.11>

- François, T., Agard, P., Bernet, M., Meyer, B., Chung, S.-L., Zarrinkoub, M. H., et al. (2014). Cenozoic exhumation of the internal Zagros: First constraints from low-temperature thermochronology and implications for the build-up of the Iranian plateau. *Lithos*, 206–207(1), 100–112. <https://doi.org/10.1016/j.lithos.2014.07.021>
- Garel, F., Goes, S., Davies, D. R., Davies, J. H., Kramer, S. C., & Wilson, C. R. (2014). Interaction of subducted slabs with the mantle transition-zone: A regime diagram from 2-D thermo-mechanical models with a mobile trench and an overriding plate. *Geochemistry, Geophysics, Geosystems*, 15, 1739–1765. <https://doi.org/10.1002/2014GC005257>
- Ghasemi, H., Juteau, T., Bellon, H., Sabzehei, M., Whitechurch, H., & Ricou, L.-E. (2002). The mafic-ultramafic complex of Sikhoran (central Iran): A polygenetic ophiolite complex. *Comptes Rendus Geoscience*, 334(6), 431–438. [https://doi.org/10.1016/s1631-0713\(02\)01770-4](https://doi.org/10.1016/s1631-0713(02)01770-4)
- Ghazi, J. M., Moazzen, M., Rahgoshay, M., & Shafaii Moghadam, H. (2012). Geochemical characteristics of basaltic rocks from the Nain ophiolite (Central Iran): Constraints on mantle wedge source evolution in an oceanic back arc basin and a geodynamical model. *Tectonophysics*, 574–575, 92–104. <https://doi.org/10.1016/j.tecto.2011.10.001>
- Green, T., Abdullayev, N., Hossack, J., Riley, G., & Roberts, A. M. (2009). Sedimentation and subsidence in the south Caspian Basin, Azerbaijan. *Geological Society Special Publication*, 312, 241–260. <https://doi.org/10.1144/SP312.12>
- Grima, A. G. (2020). *How the relationship between subduction and mantle dynamics shapes slab evolution at mid-mantle depths*. UCL (University College London).
- Guest, B., Axen, G. J., Lam, P. S., & Hassanzadeh, J. (2006a). Late Cenozoic shortening in the west-central Alborz Mountains, northern Iran, by combined conjugate strike-slip and thin-skinned deformation. *Geosphere*, 2(1), 35–52. <https://doi.org/10.1130/GES00019.1>
- Guest, B., Horton, B. K., Axen, G. J., Hassanzadeh, J., & McIntosh, W. C. (2007). Middle to late Cenozoic basin evolution in the western Alborz Mountains: Implications for the onset of collisional deformation in northern Iran. *Tectonics*, 26, TC6011. <https://doi.org/10.1029/2006TC002091>
- Guest, B., Stockli, D. F., Grove, M., Axen, G. J., Lam, P. S., & Hassanzadeh, J. (2006b). Thermal histories from the central Alborz Mountains, northern Iran: Implications for the spatial and temporal distribution of deformation in northern Iran. *Geological Society of America Bulletin*, 118(11–12), 1507–1521. <https://doi.org/10.1130/B25819.1>
- Guillaume, B., Funicello, F., Faccenna, C., Martinod, J., & Olivetti, V. (2010). Spreading pulses of the Tyrrhenian Sea during the narrowing of the Calabrian slab. *Geology*, 38(9), 819–822. <https://doi.org/10.1130/G31038.1>
- Guillaume, B., Martinod, J., & Espurt, N. (2009). Variations of slab dip and overriding plate tectonics during subduction: Insights from analogue modelling. *Tectonophysics*, 463(1–4), 167–174. <https://doi.org/10.1016/j.tecto.2008.09.043>
- Guillou-Frottier, L., Buttles, J., & Olson, P. (1995). Laboratory experiments on the structure of subducted lithosphere. *Earth and Planetary Science Letters*, 133(1–2), 19–34. [https://doi.org/10.1016/0012-821x\(95\)00045-e](https://doi.org/10.1016/0012-821x(95)00045-e)
- Gurnis, M., & Hager, B. H. (1988). Controls of the structure of subducted slabs. *Nature*, 335(22), 317–321. <https://doi.org/10.1038/335317a0>
- Gurnis, M., Hall, C., & Lavier, L. (2004). Evolving force balance during incipient subduction. *Geochemistry, Geophysics, Geosystems*, 5, Q07001. <https://doi.org/10.1029/2003GC000681>
- Gvirtzman, Z., Faccenna, C., & Becker, T. W. (2016). Isostasy, flexure, and dynamic topography. *Tectonophysics*, 683, 255–271. <https://doi.org/10.1016/j.tecto.2016.05.041>
- Hadi, M., Vahidinia, M., & Hrabovsky, J. (2019). Larger foraminiferal biostratigraphy and microfacies analysis from the Ypresian (Il-erdian-Cuisian) limestones in the Sistan Suture Zone (Eastern Iran). *Turkish Journal of Earth Sciences*, 28(1), 122–145. <https://doi.org/10.3906/yer-1802-10>
- Hassanzadeh, J., & Wernicke, B. P. (2016). The Neotethyan Sanandaj-Sirjan zone of Iran as an archetype for passive margin-arc transitions. *Tectonics*, 35, 586–621. <https://doi.org/10.1002/2015TC003926>
- Hidas, K., Booth-Rea, G., Garrido, C. J., Martínez-Martínez, J. M., Padrón-Navarta, J. A., Konc, Z., et al. (2013). Backarc basin inversion and subcontinental mantle emplacement in the crust: Kilometre-scale folding and shearing at the base of the proto-Alborán lithospheric mantle (Betic Cordillera, southern Spain). *Journal of the Geological Society*, 170(1), 47–55. <https://doi.org/10.1144/jgs2011-151>
- Houseman, G. A., & Gubbins, D. (1997). Deformation of subducted oceanic lithosphere. *Geophysical Journal International*, 131(3), 535–551. <https://doi.org/10.1111/j.1365-246x.1997.tb06598.x>
- Huismans, R., & Beaumont, C. (2011). Depth-dependent extension, two-stage breakup and cratonic underplating at rifted margins. *Nature*, 473(7345), 74–78. <https://doi.org/10.1038/nature09988>
- Hunziker, D., Burg, J.-P., Bouilhol, P., & Von Quadt, A. (2015). Jurassic rifting at the Eurasian Tethys margin: Geochemical and geochronological constraints from granitoids of North Makran, southeastern Iran. *Tectonics*, 34, 571–593. <https://doi.org/10.1002/2014TC003768>
- Jackson, J., Priestley, K., Allen, M., & Berberian, M. (2002). Active tectonics of the South Caspian basin. *Geophysical Journal International*, 148(2), 214–245. <https://doi.org/10.1046/j.1365-246X.2002.01588.x>
- Jahangiri, A. (2007). Post-collisional Miocene adakitic volcanism in NW Iran: Geochemical and geodynamic implications. *Journal of Asian Earth Sciences*, 30(3–4), 433–447. <https://doi.org/10.1016/j.jseaes.2006.11.008>
- Jamshidi, K., Ghasemi, H., Troll, V. R., Sadeghian, M., & Dahren, B. (2015). Magma storage and plumbing of adakite-type post-ophiolite intrusions in the Sabzevar ophiolitic zone, northeast Iran. *Solid Earth*, 6(1), 49–72. <https://doi.org/10.5194/se-6-49-2015>
- Jentzer, M., Fournier, M., Agard, P., Omrani, J., Khatib, M. M., & Whitechurch, H. (2017). Neogene to Present paleostress field in Eastern Iran (Sistan belt) and implications for regional geodynamics. *Tectonics*, 36, 321–339. <https://doi.org/10.1002/2016TC004275>
- Jolivet, L., Faccenna, C., Huet, B., Labrousse, L., Le Pourhiet, L., Lacombe, O., et al. (2013). Aegean tectonics: Strain localisation, slab tearing and trench retreat. *Tectonophysics*, 597–598, 1–33. <https://doi.org/10.1016/j.tecto.2012.06.011>
- Kargaranbafghi, F., Foeken, J. P. T., Guest, B., & Stuart, F. M. (2012). Cooling history of the Chapedony metamorphic core complex, Central Iran: Implications for the Eurasia-Arabia collision. *Tectonophysics*, 524–525, 100–107. <https://doi.org/10.1016/j.tecto.2011.12.022>
- Kincaid, C., & Olson, P. (1987). An experimental study of subduction and slab migration. *Journal of Geophysical Research*, 92(B13), 13832–13840. <https://doi.org/10.1029/JB092iB13p13832>
- Koshnaw, R. I., Stockli, D. F., & Schlunegger, F. (2018). Timing of the Arabia-Eurasia continental collision: Evidence from detrital zircon U-Pb geochronology of the Red Bed Series strata of the northwest Zagros hinterland, Kurdistan region of Iraq. *Geology*, 47(1), 47–50. <https://doi.org/10.1130/G46438Y.110.1130/g45499.1>
- Kurzawa, T., Bröcker, M., Fotoohi Rad, G., Berndt, J., & Lisker, F. (2017). Cretaceous high-pressure metamorphism and low pressure overprint in the Sistan Suture Zone, eastern Iran: Additional temperature estimates for eclogites, geological significance of U-Pb zircon ages and Rb-Sr constraints on the timing of exhumation. *Journal of Asian Earth Sciences*, 147, 332–344. <https://doi.org/10.1016/j.jseaes.2017.07.051>
- Lu, C., & Grand, S. P. (2016). The effect of subducting slabs in global shear wave tomography. *Geophysical Journal International*, 205, 1074–1085. <https://doi.org/10.1093/gji/ggw072>

- Lyberis, N., & Manby, G. (1999). Oblique to orthogonal convergence across the turan block in the post-Miocene. *American Association of Petroleum Geologists Bulletin*, 83(7), 1135–1160. <https://doi.org/10.1306/e4fd2e97-1732-11d7-8645000102c1865d>
- Macaud erie, J. (1983). Les roches metamorphiques au chainon ophiolitique de Sabzevar—Etude structural du domaine de Soltanabad (NE Iran). *Ophioliti*, 8, 127–128.
- Madanipour, S., Ehlers, T. A., Yassaghi, A., & Enkelmann, E. (2017). Accelerated middle Miocene exhumation of the Talesh Mountains constrained by U-Th/He thermochronometry: Evidence for the Arabia-Eurasia collision in the NW Iranian Plateau. *Tectonics*, 36, 1538–1561. <https://doi.org/10.1002/2016TC004291>
- Madanipour, S., Ehlers, T. A., Yassaghi, A., Rezaeian, M., Enkelmann, E., & Bahroudi, A. (2013). Synchronous deformation on orogenic plateau margins: Insights from the Arabia-Eurasia collision. *Tectonophysics*, 608, 440–451. <https://doi.org/10.1016/j.tecto.2013.09.003>
- Mahmoodabadi, M., Yaminifard, F., Tatar, M., & Kaviani, A. (2020). Shear wave velocity structure of the upper-mantle beneath the northern Zagros collision zone revealed by nonlinear teleseismic tomography and Bayesian Monte-Carlo joint inversion of surface wave dispersion and teleseismic P-wave coda. *Physics of the Earth and Planetary Interiors*, 300, 106444. <https://doi.org/10.1016/j.pepi.2020.106444>
- Mammadov, P. Z. (2008). The subsidence evolution of the South Caspian Basin. In EAGE International Conference on Petroleum Geology and Hydrocarbon Potential of Caspian and Black Sea Regions. <https://doi.org/10.3997/2214-4609.20146089>
- Mao, W., & Zhong, S. (2018). Slab stagnation due to a reduced viscosity layer beneath the mantle transition zone. *Nature Geoscience*, 11(11), 876–881. <https://doi.org/10.1038/s41561-018-0225-2>
- Martinod, J., Guillaume, B., Espurt, N., Faccenna, C., Funicello, F., & Regard, V. (2013). Effect of aseismic ridge subduction on slab geometry and overriding plate deformation: Insights from analogue modeling. *Tectonophysics*, 588, 39–55. <https://doi.org/10.1016/j.tecto.2012.12.010>
- Mattei, M., Cifelli, F., Alimohammadian, H., Rashid, H., Winkler, A., & Sagnotti, L. (2017). Oroclinal bending in the Alborz Mountains (Northern Iran): New constraints on the age of South Caspian subduction and extrusion tectonics. *Gondwana Research*, 42, 13–28. <https://doi.org/10.1016/j.gr.2016.10.003>
- Mattei, M., Cifelli, F., Muttoni, G., & Rashid, H. (2015). Post-Cimmerian (Jurassic-Cenozoic) paleogeography and vertical axis tectonic rotations of Central Iran and the Alborz Mountains. *Journal of Asian Earth Sciences*, 102, 92–101. <https://doi.org/10.1016/j.jseas.2014.09.038>
- Mazhari, S. A., Bea, F., Amini, S., Ghalamghash, J., Molina, J. F., Montero, P., et al. (2009). The Eocene bimodal Piranshahr massif of the Sanandaj-Sirjan Zone, NW Iran: A marker of the end of the collision in the Zagros orogen. *Journal of the Geological Society, London*, 166, 53–69. <https://doi.org/10.1144/0016-76492008-022>
- McQuarrie, N., & van Hinsbergen, D. J. J. (2013). Retrodeforming the Arabia-Eurasia collision zone: Age of collision versus magnitude of continental subduction. *Geology*, 41(3), 315–318. <https://doi.org/10.1130/G33591.1>
- Moghadam, H. S., Corfu, F., Chiaradia, M., Stern, R. J., & Ghorbani, G. (2014). Sabzevar Ophiolite, NE Iran: Progress from embryonic oceanic lithosphere into magmatic arc constrained by new isotopic and geochemical data. *Lithos*, 210–211, 224–241. <https://doi.org/10.1016/j.lithos.2014.10.004>
- Moghadam, H. S., Corfu, F., Stern, R. J., & Lotfi Bakhsh, A. (2019). The Eastern Khoy metamorphic complex of NW Iran: A Jurassic ophiolite or continuation of the Sanandaj-Sirjan Zone? *Journal of the Geological Society*, 176(3), 517–529. <https://doi.org/10.1144/jgs2018-081>
- Moghadam, H. S., Griffin, W. L., Kirchenbaur, M., Garbe-Sch onberg, D., Zakie Khedr, M., Kimura, J. -I. et al., (2018). Roll-Back, Extension and Mantle Upwelling Triggered Eocene Potassic Magmatism in NW Iran. *Journal of Petrology*, 59(7), 1417–1465. <https://doi.org/10.1093/petrology/egy067>
- Moghadam, H. S., Rossetti, F., Lucci, F., Chiaradia, M., Gerdes, A., Martinez, M. L., et al. (2016). The calc-alkaline and adakitic volcanism of the Sabzevar structural zone (NE Iran): Implications for the Eocene magmatic flare-up in Central Iran. *Lithos*, 248–251, 517–535. <https://doi.org/10.1016/j.lithos.2016.01.019>
- Moghadam, H. S., & Stern, R. J. (2015). Ophiolites of Iran: Keys to understanding the tectonic evolution of SW Asia: (II) Mesozoic ophiolites. *Journal of Asian Earth Sciences*, 100, 31–59. <http://dx.doi.org/10.1016/j.jseas.2014.12.016>
- Moghadam, H. S., Stern, R. J., Griffin, W. L., Khedr, M. Z., Kirchenbaur, M., Ottley, C. J., et al. (2020). Subduction initiation and back-arc opening north of Neo-Tethys: Evidence from the Late Cretaceous Torbat-e-Heydarieh ophiolite of NE Iran. *Bulletin of the Geological Society of America*, 132(5–6), 1083–1105. <https://doi.org/10.1130/B35065.1>
- Moghadam, H. S., Whitechurch, H., Rahgoshay, M., & Monsef, I. (2009). Significance of Nain-Baft ophiolitic belt (Iran): Short-lived, transtensional Cretaceous back-arc oceanic basins over the Tethyan subduction zone. *Comptes Rendus Geoscience*, 341(12), 1016–1028. <https://doi.org/10.1016/j.crte.2009.06.011>
- Monsef, I., Rahgoshay, M., Mohajjel, M., & Shafaii Moghadam, H. (2010). Peridotites from the Khoy Ophiolitic Complex, NW Iran: Evidence of mantle dynamics in a supra-subduction-zone context. *Journal of Asian Earth Sciences*, 38(3–4), 105–120. <https://doi.org/10.1016/j.jseas.2009.10.007>
- Moresi, L., & Gurnis, M. (1996). Constraints on the lateral strength of slabs from three-dimensional dynamic flow models. *Earth and Planetary Science Letters*, 138(1–4), 15–28. [https://doi.org/10.1016/0012-821x\(95\)00221-w](https://doi.org/10.1016/0012-821x(95)00221-w)
- Moritz, R., Ghazban, F., & Singer, B. S. (2006). Eocene gold ore formation at Muteh, Sanandaj-Sirjan tectonic zone, western Iran: A result of late-stage extension and exhumation of metamorphic basement rocks within the Zagros orogen. *Economic Geology*, 101(8), 1497–1524. <https://doi.org/10.2113/gsecongeo.101.8.1497>
- Morley, C. K., Kongwung, B., Julapour, A. A., Abdolghafourian, M., Hajian, M., Waples, D., et al. (2009). Structural development of a major late Cenozoic basin and transpressional belt in central Iran: The Central Basin in the Qom-Saveh area. *Geosphere*, 5(4), 325–362. <https://doi.org/10.1130/GES00223.1>
- Mosavinia, A., & Wilsem, M. (2011). Cenomanian acanthoceratoidea (Cretaceous Ammonoidea) from the Kopeh-Dagh, NE Iran: Taxonomy and stratigraphic implications. *Acta Geologica Polonica*, 61(2), 175–192.
- Motaghi, K., Shabaniyan, E., Tatar, M., Cuffaro, M., & Dogliani, C. (2017). The south Zagros suture zone in teleseismic images. *Tectonophysics*, 694, 292–301. <https://doi.org/10.1016/j.tecto.2016.11.012>
- Mouthereau, F. (2011). Timing of uplift in the Zagros belt/Iranian plateau and accommodation of late Cenozoic Arabia-Eurasia convergence. *Geological Magazine*, 148(5–6), 726–738. <https://doi.org/10.1017/S0016756811000306>
- Neill, I., Meliksetian, K., Allen, M. B., Navarsardyan, G., & Karapetyan, S. (2013). Pliocene-Quaternary volcanic rocks of NW Armenia: Magmatism and lithospheric dynamics within an active orogenic plateau. *Lithos*, 180–181, 200–215. <https://doi.org/10.1016/j.lithos.2013.05.005>
- Nouri, F., Azizi, H., Golonka, J., Asahara, Y., Orihashi, Y., Yamamoto, K., et al. (2016). Age and petrogenesis of Na-rich felsic rocks in western Iran: Evidence for closure of the southern branch of the Neo-tethys in the late cretaceous. *Tectonophysics*, 671, 151–172. <https://doi.org/10.1016/j.tecto.2015.12.014>

- Nozaem, R., Mohajjel, M., Rossetti, F., Della Seta, M., Vignaroli, G., Yassaghi, A., et al. (2013). Post-Neogene right-lateral strike-slip tectonics at the north-western edge of the Lut Block (Kuh-e-Sarhangi Fault), Central Iran. *Tectonophysics*, 589, 220–233. <https://doi.org/10.1016/j.tecto.2013.01.001>
- Obayashi, M., Yoshimitsu, J., Nolet, G., Fukao, Y., Shiobara, H., Sugioka, H., et al. (2013). Finite frequency whole mantle P wave tomography: Improvement of subducted slab images. *Geophysical Research Letters*, 40, 5652–5657. <https://doi.org/10.1002/2013GL057401>
- Omrani, H., Moazzen, M., Oberhänsli, R., Altenberger, U., & Lange, M. (2013). The Sabzevar blueschists of the North-Central Iranian micro-continent as remnants of the Neotethys-related oceanic crust subduction. *International Journal of Earth Sciences (Geol Rundsch)*, 102(5), 1491–1512. <https://doi.org/10.1007/s00531-013-0881-9>
- Omrani, J., Agard, P., Whitechurch, H., Benoit, M., Prouteau, G., & Jolivet, L. (2008). Arc-magmatism and subduction history beneath the Zagros Mountains, Iran: A new report of adakites and geodynamic consequences. *Lithos*, 106(3–4), 380–398. <https://doi.org/10.1016/j.lithos.2008.09.008>
- Paknia, M., Ballato, P., Heidarzadeh, G., Cifelli, F., Hassanzadeh, J., Vezzoli, G. et al. (2021). Neogene Tectono-Stratigraphic Evolution of the Intermontane Tarom Basin: Insights Into Basin Filling and Plateau Building Processes Along the Northern Margin of the Iranian Plateau (Arabia-Eurasia Collision Zone). *Tectonics*, 40(3), <https://doi.org/10.1029/2020tc006254>
- Pang, K.-N., Chung, S.-L., Zarrinkoub, M. H., Chiu, H.-Y., & Li, X.-H. (2014). On the magmatic record of the Makran arc, southeastern Iran: Insights from zircon U-Pb geochronology and bulk-rock geochemistry. *Geochemistry, Geophysics, Geosystems*, 15, 2151–2169. <https://doi.org/10.1002/2014GC005262>
- Pang, K.-N., Chung, S.-L., Zarrinkoub, M. H., Khatib, M. M., Mohammadi, S. S., Chiu, H.-Y., et al. (2013). Eocene-Oligocene post-collisional magmatism in the Lut-Sistan region, eastern Iran: Magma genesis and tectonic implications. *Lithos*, 180–181, 234–251. <https://doi.org/10.1016/j.lithos.2013.05.009>
- Pang, K.-N., Chung, S.-L., Zarrinkoub, M. H., Li, X.-H., Lee, H.-Y., Lin, T.-H., & Chiu, H.-Y. (2016). New age and geochemical constraints on the origin of Quaternary adakite-like lavas in the Arabia-Eurasia collision zone. *Lithos*, 264, 348–359. <https://doi.org/10.1016/j.lithos.2016.08.042>
- Paul, A., Hatzfeld, D., Kaviani, A., Tatar, M., Péquegnat, C., Hatzfeld, D., et al. (2010). Seismic imaging of the lithospheric structure of the Zagros mountain belt (Iran). *Geological Society, London, Special Publications*, 330, 5–18. <https://doi.org/10.1144/SP330.2>
- Paul, A., Kaviani, A., Hatzfeld, D., Vergne, J., & Mokhtari, M. (2006). Seismological evidence for crustal-scale thrusting in the Zagros mountain belt (Iran). *Geophysical Journal International*, 166, 227–237. <https://doi.org/10.1111/j.1365-246X.2006.02920.x>
- Pirnia, T., Saccani, E., & Arai, S. (2018). Spinel and plagioclase peridotites of the Nain ophiolite (Central Iran): Evidence for the incipient stage of oceanic basin formation. *Lithos*, 310–311, 1–19. <https://doi.org/10.1016/j.lithos.2018.04.001>
- Pirnia, T., Saccani, E., Torabi, G., Chiari, M., Goričan, Š., & Barbero, E. (2020). Cretaceous tectonic evolution of the Neo-Tethys in Central Iran: Evidence from petrology and age of the Nain-Ashin ophiolitic basalts. *Geoscience Frontiers*, 11(1), 57–81. <https://doi.org/10.1016/j.gsf.2019.02.008>
- Pirouz, M., Avouac, J.-P., Hassanzadeh, J., Kirschvink, J. L., & Bahroudi, A. (2017). Early Neogene foreland of the Zagros, implications for the initial closure of the Neo-Tethys and kinematics of crustal shortening. *Earth and Planetary Science Letters*, 477, 168–182. <https://doi.org/10.1016/j.epsl.2017.07.046>
- Pirouz, M., Simpson, G., & Chiaradia, M. (2015). Constraint on foreland basin migration in the Zagros mountain belt using Sr isotope stratigraphy. *Basin Research*, 27(6), 714–728. <https://doi.org/10.1111/bre.12097>
- Priestley, K., Mckenzie, D., Barron, J., Tatar, M., & Debayle, E. (2012). The Zagros core: Deformation of the continental lithospheric mantle. *Geochemistry, Geophysics, Geosystems*, 13, Q11014. <https://doi.org/10.1029/2012GC004435>
- Rabiee, A., Rossetti, F., Asahara, Y., Azizi, H., Lucci, F., Lustrino, M., & Nozaem, R. (2020). Long-lived, Eocene-Miocene stationary magmatism in NW Iran along a transform plate boundary. *Gondwana Research*, 85, 237–262. <https://doi.org/10.1016/j.gr.2020.03.014>
- Rahmani, M., Motaghi, K., Ghods, A., Sobouti, F., Talebian, M., Ai, Y., & Chen, L. (2019). Deep velocity image of the north Zagros collision zone (Iran) from regional and teleseismic tomography. *Geophysical Journal International*, 219(3), 1729–1740. <https://doi.org/10.1093/gji/ggz393>
- Rezaeian, M., Carter, A., Hovius, N., & Allen, M. B. (2012). Cenozoic exhumation history of the Alborz Mountains, Iran: New constraints from low-temperature chronometry. *Tectonics*, 31(2), <https://doi.org/10.1029/2011tc002974>
- Ribe, N. M., Stutzmann, E., Ren, Y., & van der Hilst, R. (2007). Buckling instabilities of subducted lithosphere beneath the transition zone. *Earth and Planetary Science Letters*, 254(1–2), 173–179. <https://doi.org/10.1016/j.epsl.2006.11.028>
- Ritsema, J., Deuss, A., Van Heijst, H. J., & Woodhouse, J. H. (2011). S4ORTS: A degree-40 shear-velocity model for the mantle from new Rayleigh wave dispersion, teleseismic traveltimes and normal-mode splitting function measurements. *Geophysical Journal International*, 184(3), 1223–1236. <https://doi.org/10.1111/j.1365-246X.2010.04884.x>
- Robert, A. M. M., Letouzey, J., Kavooosi, M. A., Müller, C., Vergés, J., & Aghababaei, A. (2014). Structural evolution of the Kopeh Dagh fold-and-thrust belt (NE Iran) and interactions with the South Caspian Sea Basin and Amu Darya Basin. *Marine and Petroleum Geology*, 57, 68–87.
- Rossetti, F., Nasrabad, M., Theye, T., Gerdes, A., Monié, P., Lucci, F., & Vignaroli, G. (2014). Adakite differentiation and emplacement in a subduction channel: The late paleocene Sabzevar magmatism (NE Iran). *Geological Society of America Bulletin*, 126(3–4), 317–343. <https://doi.org/10.1130/B30913.1>
- Rossetti, F., Nasrabad, M., Vignaroli, G., Theye, T., Gerdes, A., Razavi, M. H., & Vaziri, H. M. (2010). Early Cretaceous migmatitic mafic granulites from the Sabzevar range (NE Iran): Implications for the closure of the Mesozoic peri-Tethyan oceans in central Iran. *Terra Nova*, 22(1), 26–34. <https://doi.org/10.1111/j.1365-3121.2009.00912.x>
- Saccani, E., Allahyari, K., & Rahimzadeh, B. (2014). Petrology and geochemistry of mafic magmatic rocks from the Sarve-Abad ophiolites (Kurdistan region, Iran): Evidence for interaction between MORB-type asthenosphere and OIB-type components in the southern Neo-Tethys Ocean. *Tectonophysics*, 621, 132–147. <https://doi.org/10.1016/j.tecto.2014.02.011>
- Saccani, E., Delavari, M., Beccaluva, L., & Amini, S. (2010). Petrological and geochemical constraints on the origin of the Nehbandan ophiolitic complex (eastern Iran): Implication for the evolution of the Sistan Ocean. *Lithos*, 117(1–4), 209–228. <https://doi.org/10.1016/j.lithos.2010.02.016>
- Saidi, A., Brunet, M.-F., & Ricou, L.-E. (1997). Continental accretion of the Iran block to Eurasia as seen from late Paleozoic to early cretaceous subsidence curves. *Geodinamica Acta*, 10(5), 189–208. <https://doi.org/10.1080/09853111.1997.11105302>
- Sepahi, A. A., & Athari, S. F. (2006). Petrology of major granitic plutons of the northwestern part of the Sanandaj-Sirjan Metamorphic Belt, Zagros Orogen, Iran: With emphasis on A-type granitoids from the SE Saqqez area. *Neues Jahrbuch Fur Mineralogie, Abhandlungen*, 183(1), 93–106. <https://doi.org/10.1127/0077-7757/2006/0063>

- Seton, M., Müller, R. D., Zahirovic, S., Gaina, C., Torsvik, T., Shephard, G., et al. (2012). Global continental and ocean basin reconstructions since 200Ma. *Earth-Science Reviews*, *113*(3–4), 212–270. <https://doi.org/10.1016/j.earscirev.2012.03.002>
- Shababian, E., Acocella, V., Gioncada, A., Ghasemi, H., & Bellier, O. (2012). Structural control on volcanism in intraplate post collisional settings: Late Cenozoic to Quaternary examples of Iran and Eastern Turkey. *Tectonics*, *31*, TC3013. <https://doi.org/10.1029/2011TC003042>
- Shojaat, B., Hassanipak, A. A., Mobasher, K., & Ghazi, A. M. (2003). Petrology, geochemistry and tectonics of the Sabzevar ophiolite, North Central Iran. *Journal of Asian Earth Sciences*, *21*(9), 1053–1067. [https://doi.org/10.1016/s1367-9120\(02\)00143-8](https://doi.org/10.1016/s1367-9120(02)00143-8)
- Stampfli, G. M., & Borel, G. D. (2002). A plate tectonic model for the Paleozoic and Mesozoic constrained by dynamic plate boundaries and restored synthetic oceanic isochrons. *Earth and Planetary Science Letters*, *196*(1–2), 17–33. [https://doi.org/10.1016/s0012-821x\(01\)00588-x](https://doi.org/10.1016/s0012-821x(01)00588-x)
- Stöcklin, J. (1968). Structural history and tectonics of Iran: A review. *American Association of Petroleum Geologists Bulletin*, *52*(7), 1229–1258.
- Tadayon, M., Rossetti, F., Zattin, M., Calzolari, G., Nozaem, R., Salvini, F., et al. (2019). The long-term evolution of the Doruneh Fault region (Central Iran): A key to understanding the spatio-temporal tectonic evolution in the hinterland of the Zagros convergence zone. *Geological Journal*, *54*(3), 1454–1479. <https://doi.org/10.1002/gj.3241>
- Tadayon, M., Rossetti, F., Zattin, M., Nozaem, R., Calzolari, G., Madanipour, S., & Salvini, F. (2017). The post-Eocene evolution of the Doruneh fault region (Central Iran): The intraplate response to the reorganization of the Arabia-Eurasia collision zone. *Tectonics*, *36*, 3038–3064. <https://doi.org/10.1002/2017TC004595>
- Taylor, B., & Karner, G. D. (1983). On the evolution of marginal basins. *Reviews of Geophysics*, *21*(8), 1727–1741. <https://doi.org/10.1029/RG021i008p01727>
- van der Meer, D. G., van Hinsbergen, D. J. J., & Spakman, W. (2018). Atlas of the underworld: Slab remnants in the mantle, their sinking history, and a new outlook on lower mantle viscosity. *Tectonophysics*, *723*, 309–448. <https://doi.org/10.1016/j.tecto.2017.10.004>
- Van Der Voo, R., Spakman, W., & Bijwaard, H. (2000). Tethyan subducted slabs under India. *Earth and Planetary Science Letters*, *171*(1), 7–20. [https://doi.org/10.1016/S0012-821X\(99\)00131-4](https://doi.org/10.1016/S0012-821X(99)00131-4)
- Vaziri, S. H., Fürsich, F. T., & Kohansal-ghadimvand, N. (2012). Facies analysis and depositional environments of the Upper Cretaceous Sadr unit in the Nakhlak area, Central Iran. *Revista Mexicana de Ciencias Geológicas*, *29*(2), 384–397.
- Verdel, C., Wernicke, B. P., Hassanzadeh, J., & Guest, B. (2011). A Paleogene extensional arc flare-up in Iran. *Tectonics*, *30*, TC3008. <https://doi.org/10.1029/2010TC002809>
- Verdel, C., Wernicke, B. P., Ramezani, J., Hassanzadeh, J., Renne, P. R., & Spell, T. L. (2007). Geology and thermochronology of Tertiary Cordilleran-style metamorphic core complexes in the Saghand region of central Iran. *Geological Society of America Bulletin*, *119*(7–8), 961–977. <https://doi.org/10.1130/B26102.1>
- Wang, H., Agrusta, R., & van Hunen, J. (2015). Advantages of a conservative velocity interpolation (CVI) scheme for particle-in-cell methods with application in geodynamic modeling. *Geochemistry, Geophysics, Geosystems*, *16*, 2015–2023. <https://doi.org/10.1002/2015GC005824>
- Wilmsen, M., Berensmeier, M., Fürsich, F. T., Majidifard, M. R., & Schlagintweit, F. (2018). A late cretaceous epeiric carbonate platform: The Haftoman formation of central Iran. *Facies*, *64*(2), 11. <https://doi.org/10.1007/s10347-018-0523-6>
- Wilmsen, M., Fürsich, F. T., & Majidifard, M. R. (2015). An overview of the Cretaceous stratigraphy and facies development of the Yazd Block, western Central Iran. *Journal of Asian Earth Sciences*, *102*, 73–91. <https://doi.org/10.1016/j.jseaes.2014.07.015>
- Wilmsen, M., Fürsich, F. T., Seyed-Emami, K., & Majidifard, M. R. (2009). An overview of the stratigraphy and facies development of the Jurassic System on the Tabas Block, east-central Iran. *Geological Society London Special Publication*, *312*, 323–343. <https://doi.org/10.1144/SP312.15>
- Wilmsen, M., Wiese, F., Seyed-Emami, K., & Fürsich, F. T. (2005). First record and significance of Turonian ammonites from the Shotori Mountains, east-central Iran. *Cretaceous Research*, *26*(2), 181–195. <https://doi.org/10.1016/j.cretres.2004.10.004>
- Wortel, M. J. R., & Spakman, W. (2000). Subduction and slab detachment in the Mediterranean-Carpathian region. *Science*, *290*(5498), 1910–1917. <https://doi.org/10.1126/science.290.5498.1910>
- Yang, T., Gurnis, M., & Zahirovic, S. (2016). Mantle-induced subsidence and compression in SE Asia since the early Miocene. *Geophysical Research Letters*, *43*, 1901–1909. <https://doi.org/10.1002/2016GL068050>
- Yang, T., Gurnis, M., & Zahirovic, S. (2018). Slab avalanche-induced tectonics in self-consistent dynamic models. *Tectonophysics*, *746*, 251–265. <https://doi.org/10.1016/j.tecto.2016.12.007>
- Zanchi, A., Berra, F., Mattei, M., Ghassemi, M. R., & Sabouri, J. (2006). Inversion tectonics in central Alborz, Iran. *Journal of Structural Geology*, *28*(11), 2023–2037. <https://doi.org/10.1016/j.jsg.2006.06.020>
- Zanchi, A., Zanchetta, S., Garzanti, E., Balini, M., Berra, F., Mattei, M., & Muttoni, G. (2009). The Cimmerian evolution of the Nakhlak-Anarak area, Central Iran, and its bearing for the reconstruction of the history of the Eurasian margin. *Geological Society, London, Special Publications*, *312*, 261–286. <https://doi.org/10.1144/SP312.13>
- Zarrinkoub, M. H., Pang, K.-N., Chung, S.-L., Khatib, M. M., Mohammadi, S. S., Chiu, H.-Y., et al. (2012). Zircon U-Pb age and geochemical constraints on the origin of the Birjand ophiolite, Sistan suture zone, eastern Iran. *Lithos*, *154*, 392–405. <https://doi.org/10.1016/j.lithos.2012.08.007>
- Zhong, S., & Gurnis, M. (1994). Controls on trench topography from dynamic models of subducted slabs. *Journal of Geophysical Research*, *99*(B8), 683–695. <https://doi.org/10.1029/94JB00809>